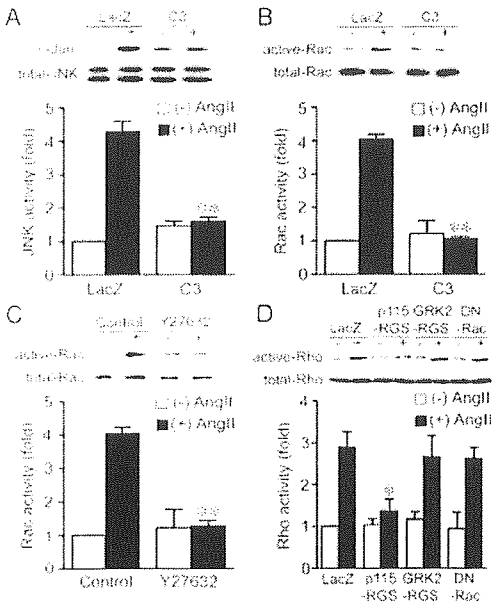

FIG. 8. **Rho-mediated activation of JNK and Rac.** Cardiac myocytes were infected with adenovirus expressing C3 toxin. The cells were then stimulated with Ang II (100 nM) for 20 min (JNK activation) or 1 min (Rac activation), and JNK activity (*A*) and Rac activation (*B*) were determined. *C*, cardiac myocytes were treated with a ROCK inhibitor Y27632 (10 μM) for 30 min. The cells were then stimulated with Ang II (100 nM) for 1 min, and Rac activation was determined. The fold activation was calculated by the values of untreated cells infecting with LacZ set as 1. **, $p < 0.01$ *versus* Ang II stimulation of control (LacZ-expressing) cells. *D*, cells were infected with adenovirus encoding p115-RGS, GRK2-RGS, or DN-Rac. The cells were then stimulated with Ang II (100 nM) for 1 min, and Rho activation was determined. *, $p < 0.05$ *versus* Ang II stimulation of LacZ-expressing cells. The experiments were repeated three to four times.

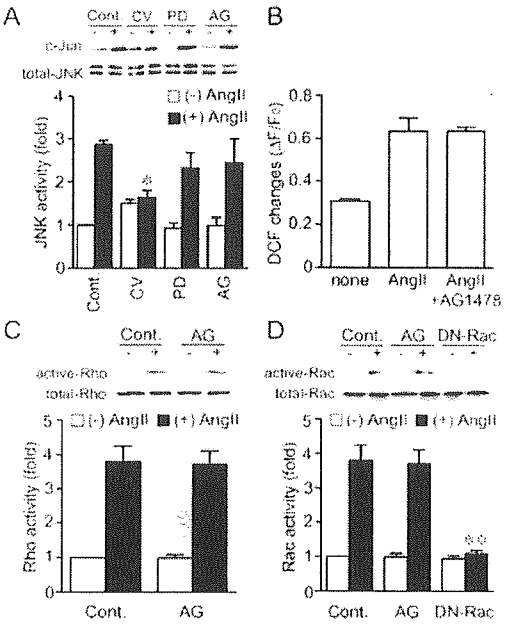

FIG. 9. **Effects of Ang II receptor subtype selective blockers or EGF receptor kinase inhibitor on Ang II-induced JNK activation cascade.** *A*, cells were treated with CV11974 (*CV*, 1 μM), PD123319 (*PD*, 5 μM), or AG1478 (*AG*, 500 nM) for 20 min before the addition of Ang II (100 nM, 20 min), and JNK activation was determined. *, $p < 0.05$ *versus* Ang II stimulation of control cells (*Cont.*). *B*, effect of an EGF receptor kinase inhibitor AG1478 on Ang II-induced ROS production. The cells were treated with AG1478 (500 nM) for 20 min before the addition of Ang II (100 nM, 25 min), and ROS production was measured. *C*, effect of AG1478 on Ang II-induced Rho activation. The cells were stimulated with Ang II (100 nM) for 1 min, and Rho activation was determined by pull-down assay. The fold activation was calculated by the values of untreated cells (control) set as 1. *D*, effect of AG1478 or DN-Rac on Ang II-induced Rac activation. The cells were infected with DN-Rac at 300 MOI or treated with AG1478 (500 nM, 20 min), and Rac activation was determined by pull-down assay. **, $p < 0.01$ *versus* Ang II stimulation of control cells. The experiments were repeated three times.

tion was significantly inhibited by CV11974 (a selective AT1R blocker), but not by PD123319 (a selective AT2R blocker), indicating that JNK was activated by type 1 subtype of ATR (Fig. 9*A*). It has been reported that EGF receptor transactivation plays an important role in G protein-coupled receptor-induced MAPK activation including AT1R (7). To examine the involvement of EGF receptor transactivation, we used an inhibitor of EGF receptor kinase AG1478. AG1478 did not affect Ang II-stimulated $G\alpha_{13}$ activation (Fig. 3*B*), JNK activation, ROS production, Rho activation, and Rac activation (Fig. 9). DN-Rac inhibited Rac activation, validating the assay method (Fig. 9*D*). These results suggest that EGF receptor is not involved in Ang II-induced JNK activation through $G\alpha_{12/13}$-mediated Rho/ROCK activation in cardiac myocytes.

DISCUSSION

We demonstrated in the present study that Ang II-induced JNK/p38 MAPK activation was mediated by a ROS-dependent signal transduction pathway: Ang II → AT1R → $G\alpha_{12/13}$ → Rho → ROCK → Rac → ROS → JNK/p38 MAPK (Fig. 10). We clearly demonstrate that ROS are produced by $G\alpha_{12/13}$-mediated Rac activation, and ROS participate in JNK and p38 MAPK but not ERK activation. Previous findings indicated that Ang II stimulation produces ROS in vascular smooth muscle cells (6, 17) and suggested the role of ROS as a mediator of Ang II action (6, 14). The present study is consistent with the reports that ROS are mediators of Ang II action. We further demonstrated that the possible origin of Ang II-induced ROS production in neonatal cardiac myocytes is NADPH oxidase, because a selective inhibitor of NADPH oxidase could inhibit ROS-dependent JNK and p38 MAPK activation by Ang II stimulation.

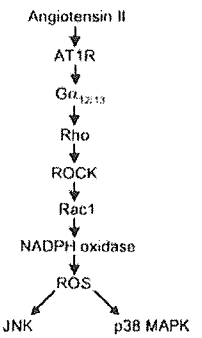

FIG. 10. **Model for ROS-dependent activation of JNK and p38 MAPK by AT1R stimulation in rat neonatal cardiac myocytes.** AT1R stimulation by angiotensin II activates $G\alpha_{12/13}$ protein. The activated $G\alpha_{12/13}$ stimulates ROS production through Rho/ROCK-mediated Rac1 activation. ROS activate JNK and p38 MAPK through with unknown mechanisms.

The expression of CA-$G\alpha_{12}$ and CA-$G\alpha_{13}$ activates all three MAPKs in rat cardiac myocytes (Fig. 5). This result is partly supported by the report that $G\alpha_{12}$ activates JNK specifically through the stimulation of MKK7, an upstream kinase of JNK (39). Furthermore, CA-$G\alpha_{12}$- or CA-$G\alpha_{13}$-induced activation of JNK and p38 MAPK was inhibited by DPI (an NADPH oxidase inhibitor). Because Ang II-induced JNK and p38 MAPK activation was significantly inhibited by catalase (an H_2O_2-degrading enzyme), we speculate the activation scheme that NADPH

oxidase-generated superoxide anion is converted to H_2O_2, and H_2O_2 forms more reactive species that participate in JNK and p38 MAPK activation machinery.

A selective EGF receptor kinase blocker AG1478 demonstrates that AT1R-stimulated JNK activation does not requires EGF receptor transactivation (Fig. 9). With cardiac fibroblasts, Murasawa *et al.* (40) reported that Ang II activates JNK through Pyk, Src, Rac, and PAK. In contrast with JNK activation, ERK activation in cardiac fibroblasts requires EGF receptor transactivation through Pyk2 and Src activation. The present study using cardiac myocytes demonstrated that Ang II-induced JNK activation was not inhibited by AG1478. We further demonstrated that Ang II-induced $G\alpha_{13}$ activation, Rho activation, Rac activation, and ROS production were not inhibited by AG1478 (Figs. 3*B* and 9). These results suggest that EGF receptor transactivation is not necessary for Ang II-induced JNK and p38 MAPK activation through $G\alpha_{12/13}$-mediated ROS production.

The present study demonstrated that Rho and ROCK positively regulate Rac activation. On the other hand, the negative regulation of Rac by Rho and ROCK has been observed by Hirose *et al.* (41). They reported that Rho/ROCK stimulated neurite retraction, and Cdc42/Rac stimulated neurite outgrowth in NIE-115 cells. They suggested that Rho/ROCK negatively regulated the Cdc42 and Rac pathway. The differential regulatory mechanism of Rac by Rho/ROCK is unknown. However, different types of RacGEF that are regulated by ROCK may express in NIE-115 and cardiac myocytes. Because we also found that a ROCK inhibitor Y27632 inhibited Ang II-induced ROS production (data not shown), the present study also suggests that ROCK mediates Ang II-induced JNK and p38 MAPK activation through Rac activation.

When cells were treated with PTX, the active form of Rac was increased even in the absence of agonist stimulation (Fig. 7*D*). The mechanism of high Rac activity by PTX treatment is unknown. One of possibilities may be mitogenic action of PTX. PTX is an A-B toxin; A-protomer is the entity that ADP-ribosylates $G\alpha_i$, and B-oligomer consists of several subunits that bind to the plasma membrane. PTX binds to cells via B-oligomer, and B-oligomer has a mitogenic activity. Therefore, the increased basal Rac activation may be caused by the mitogenic action of PTX.

DN-Rac inhibited Ang II-induced ROS production and activation of JNK and p38 MAPK. The reagents that inhibit ROS production blocked JNK and p38 MAPK activation. Thus, Rac-mediated JNK and p38 MAPK activation requires ROS. However, Rac is believed to be involved in various signaling pathways other than ROS production system (NADPH oxidase). For instance, Rac is an activator of PAK leading to JNK activation (20). We speculate that Rac activates at least two signaling pathways such as ROS production and PAK activation, and concomitant activation of two pathways is required for JNK and p38 MAPK activation.

The idea that $G_{12/13}$ proteins are involved in Ang II-mediated signaling has been also supported by some previous reports (42, 43). For example, Gohla *et al.* (42) have reported that angiotensin II stimulation increases the incorporation of azidoanilido [α-^{32}P]GTP into $G\alpha_{12}$ and $G\alpha_{13}$ in membranes of aortic smooth muscle cells. The present study substantiated their result that AT1R can directly activate $G\alpha_{13}$. We further demonstrated that inhibition of EGF receptor or $G\alpha_q$ did not affect Ang II-stimulated $G\alpha_{13}$ activation. Macrez *et al.* (43) also reported that a $\beta\gamma$ dimmer derived from G_{13} transduces AT1R signaling. Because the $\beta\gamma$-sequestering peptide GRK2-ct did not affect Ang II-induced Rac activation (Fig. 7*D*), $\beta\gamma$ derived from $G_{12/13}$ may not participate in JNK and p38 MAPK activation induced by Ang II.

$G\alpha_q$ is generally thought to mediate Ang II-induced responses. We demonstrated that expression of CA-$G\alpha_q$ activates three MAPKs in rat neonatal cardiomyocytes. However, the present study did not reveal any role of $G\alpha_q$ in Ang II receptor-stimulated JNK and p38 MAPK activation. Zou *et al.* (44) have reported that $G\alpha_q$ and protein kinase C mediate Ang II-induced ERK activation in rat cardiac myocytes. Therefore, it is reasonable to assume that the mechanism of Ang II-induced MAPK activation is different between three MAPKs; $G\alpha_q$ mediates mainly ERK activation, and $G\alpha_{12/13}$ mediates JNK and p38 MAPK activation. The blockade of JNK or p38 MAPK activation resulted in complete inhibition of Ang II-induced hypertrophic responses (32, 45). Therefore, it may be necessary to turn on multiple pathways at the same time for the full induction of hypertrophic responses upon Ang II receptor stimulation.

In summary, we have demonstrated a new signal transduction pathway of Ang II-induced JNK and p38 MAPK activation: AT1R → $G_{12/13}$ → Rho/ROCK → Rac → ROS → JNK and p38 MAPK. The signaling connection between $G\alpha_{12/13}$ and ROS in cardiac myocytes will provide a new direction of Ang II receptor-mediated signaling pathway.

Acknowledgments—We thank Drs. R. J. Lefkowitz, S. G. Rhee, K. Kaibuchi, S. Narumiya, H. Nishina, M. Simon, and M. Negishi for cDNAs encoding GRK2, PrxII, DN-Rac, C3 toxin, GST-c-Jun, $G\alpha_{12}$, $G\alpha_{13}$, and GST-TPR, respectively.

REFERENCES

1. Paradis, P., Dali-Youcef, N., Paradis, F. W., Thibault, G., and Nemer, M. (2000) *Proc. Natl. Acad. Sci. U. S. A.* **97,** 931–936
2. Schmitz, U., and Berk, B. C. (1997) *Trends. Endocrinol. Metab.* **8,** 261–266
3. Kudoh, S., Komuro, I., Mizuno, T., Yamazaki, T., Zou, Y., Shiojima, I., Takekoshi, N., and Yazaki, Y. (1997) *Circ. Res.* **80,** 139–146
4. Sadoshima, J., Qiu, Z., Morgan, J. P., and Izumo, S. (1995) *Circ. Res.* **76,** 1–15
5. Li, X., Lee, J. W., Graves, L. M., and Earp, H. S. (1998) *EMBO J.* **17,** 2574–2583
6. Ushio-Fukai, M., Alexander, R. W., Akers, M., and Griendling, K. K. (1998) *J. Biol. Chem.* **273,** 15022–15029
7. Eguchi, S., Dempsey, P. J., Frank, G. D., Motley, E. D., and Inagami, T. (2001) *J. Biol. Chem.* **276,** 7957–7962
8. Bogoyevitch, M. A., Glennon, P. E., Andersson, M. B., Clerk, A., Lazou, A., Marshall, C. J., Parker, P. J., and Sugden, P. H. (1994) *J. Biol. Chem.* **269,** 1110–1119
9. Sugden, P. H., and Clerk, A. (1998) *J. Mol. Med.* **76,** 725–746
10. Sadoshima, J., and Izumo, S. (1996) *EMBO J.* **15,** 775–787
11. Luttrell, L. M., Roudabush, F. L., Choy, E. W., Miller, W. E., Field, M. E., Pierce, K. L., and Lefkowitz, R. J. (2001) *Proc. Natl. Acad. Sci. U. S. A.* **98,** 2449–2454
12. Abe, J., and Berk, B. C. (1998) *Trends. Cardiovasc. Med.* **8,** 59–64
13. Takemoto, M. Node, K. Nakagami, H. Liao, Y. Grimm, M., Takemoto, Y., Kitakaze, M., and Liao, J. K. (2001) *J. Clin. Investig.* **108,** 1429–1437
14. Griendling, K. K., and Ushio-Fukai, M. (2000) *Regul. Pept.* **91,** 21–27
15. Nishida, M., Maruyama, Y., Tanaka, R., Kontani, K., Nagao, T., and Kurose, H. (2000) *Nature* **408,** 492–495
16. Nishida, M., Schey, K. L., Takagahara, S., Kontani, K., Katada, T., Urano, Y., Nagano, T., Nagao, T., and Kurose, H. (2002) *J. Biol. Chem.* **277,** 9036–9042
17. Rajagopalan, S., Kurz, S., Münzel, T., Tarpey, M., Freeman, B. A., Griendling, K. K., and Harrison, D. G. (1996) *J. Clin. Investig.* **97,** 1916–1923
18. Griendling, K. K., Minieri, C. A., Ollerenshaw, J. D., and Alexander, R. W. (1994) *Circ. Res.* **74,** 1141–1148
19. Bokoch, G. M., and Knaus, U. G. (2003) *Trends Biochem. Sci.* **28,** 502–508
20. Schmitzs, U., Thömmes, K., Beier, I., Wagner, W., Sachinidis, A., Düsing, R., and Vetter, H. (2001) *J. Biol. Chem.* **276,** 22003–22010
21. Nishida, M., Nagao, T., and Kurose, H. (1999) *Biochem. Biophys. Res. Commun.* **262,** 350–354
22. Coso, O. A., Chiariello, M., Yu, J.-C., Teramoto, H., Crespo, P., Xu, N., Miki, T., and Gutkind, J. S. (1995) *Cell* **81,** 1137–1146
23. Minden, A., Lin, A., McMahon, M., Lange-Carter, C. Dérijard. B., Davis, R. J., Johnson, G. L., and Karin M. (1994) *Science* **266,** 1719–1723
24. Minden, A., Lin, A., Claret, F.-X., Abo, A., and Karin, M. (1995) *Cell* **81,** 1147–1157
25. Kurose, H. (2003) *Life Sci.* **74,** 155–161
26. Kozasa, T., Jiang, X., Hart, M. J., Sternweis, P. M., Singer, W. D., Gilman, A. G., Bollag, G., and Sternweis, P. C. (1998) *Science* **280,** 2109–2111
27. Hart, M. J., Jiang, X., Kozasa, T., Roscoe, W., Singer W. D., Gilman, A. G., Sternweis, P. C., and Bollag, G. (1998) *Science* **280,** 2112–2114
28. Shiina, T., Arai, K., Tanabe, S., Yoshida, N., Haga, T., Nagao, T., and Kurose, H. (2001) *J. Biol. Chem.* **276,** 33019–33026
29. Kurose, H., Arriza, J. L., and Lefkowitz, R. J. (1993) *Mol. Pharmacol.* **43,** 444–450
30. He, T.-C., Zhou, S., Da Costa, L. T., Yu, J., Kinzler, K. W., and Vogelstein, B. (1998) *Proc. Natl. Acad. Sci. U. S. A.* **95,** 2509–2514
31. Miyake, S., Makimura, M., Kanegae, Y., Harada, S., Sato, Y., Takamori, K.,

Tokuda, C., and Saito, I. (1996) *Proc. Natl. Acad. Sci. U. S. A.* **93,** 1320–1324
32. Maruyama, Y., Nishida, M., Sugimoto, Y., Tanabe, S., Turner, J. H., Kozasa, T., Wada, T., Nagao, T., and Kurose, H. (2002) *Circ. Res.* **91,** 961–969
33. Arai, K., Maruyama, Y., Nishida, M., Tanabe, S., Takagahara, S., Kozasa, T., Mori, Y., Nagao, T., and Kurose, H. (2003) *Mol. Pharmacol.* **63,** 478–488
34. Kang, S. W., Chae, H. Z., Seo, M. S., Kim, K., Baines, I. C., and Rhee, S. G. (1998) *J. Biol. Chem.* **273,** 6297–6302
35. Ren, X.-D., and Schwartz, M. A. (2000) *Methods Enzymol.* **325,** 264–272
36. Yamaguchi, Y., Katoh, H., and Negishi, M. (2003) *J. Biol. Chem.* **278,** 14936–14939
37. Clerk, A., Pham, F. H., Fuller, S. J., Sahai, E., Aktories, K., Marais, R., Marshall, C., and Sugden, P. H. (2001) *Mol. Cell. Biol.* **21,** 1173–1184
38. Matsui, T., Amano, M., Yamamoto, T., Chihara, K., Nakafuku, M., Ito, M., Nakano, T., Okawa, K., Iwamatsu, A., and Kaibuchi, K. (1996) *EMBO J.* **15,** 2208–2216
39. Dermott, J. M., Ha, J. H., Lee, C. H., and Dhanasekaran, N. (2004) *Oncogene* **23,** 226–232
40. Murasawa, S., Matsubara, H., Mori, Y., Masaki, H., Tsutsumi, Y., Shibasaki, Y., Kitabayashi, I., Tanaka, Y., Fujiyama, S., Koyama, Y., Fujiyama, A., Iba, S., and Iwasaka, T. (2000) *J. Biol. Chem.* **275,** 26856–26863
41. Hirose, M. Ishizaki, T. Watanabe, N., Uehata, M., Kranenburg, O., Moolenaar, W. H., Matsumura, F., Maekawa, M., Bito, H., and Narumiya, S. (1998) *J. Cell Biol.* **141,** 1625–1636
42. Gohla, A., Schultz, G., and Offermanns, S. (2000) *Circ. Res.* **87,** 221–227
43. Macrez, N., Morel, J-L., Kalkbrenner, F., Viard, P., Schultz, G., and Mironneau, J. (1997) *J. Biol. Chem.* **272,** 23180–23185
44. Zou, Y., Komuro, I., Yamazaki, T., Kudoh, S., Aikawa, R., Zhu, W., Shiojima, I., Hiroi, Y., Tobe, K., Kadowaki, T., and Yazaki, Y. (1998) *Circ. Res.* **82,** 337–345
45. Reddy, M. A., Thimmalapura, P.-R., Lanting, L., Nadler, J., L., Fatima, S., and Natarajan, R. (2002) *J. Biol. Chem.* **277,** 9920–9928

Biol. Pharm. Bull. **28**(3) 424—428 (2005) Vol. 28, No. 3

Expression of Annexin A3 in Primary Cultured Parenchymal Rat Hepatocytes and Inhibition of DNA Synthesis by Suppression of Annexin A3 Expression Using RNA Interference

Shingo NIIMI,*[a] Mizuho HARASHIMA,[b] Masaru GAMOU,[b] Masashi HYUGA,[a] Taiichiro SEKI,[b] Toyohiko ARIGA,[b] Toru KAWANISHI,[a] and Takao HAYAKAWA[c]

[a] *Division of Biological Chemistry and Biologicals, National Institute of Health Sciences; 1–18–1 Kamiyoga, Setagaya-ku, Tokyo 158–8501, Japan:* [b] *Department of Nutrition and Physiology, Nihon University College of Bioresource Sciences; Kameino, Fujisawa 252–8510, Japan: and* [c] *Deputy Director General, National Institute of Health Sciences; 1–18–1 Kamiyoga, Setagaya-ku, Tokyo 158–8501, Japan.*

Received October 30, 2004; accepted January 5, 2005; published online January 7, 2005

Annexin A3 is a member of the lipocortin/annexin family, which binds to phospholipids and membranes in a Ca^{2+}-dependent manner. Although annexin A3 has various functions *in vitro*, its cellular significance is completely unknown. Annexin A3 is not found in rat liver *in vivo*. In the present study, we investigated the expression of annexin A3 in primary cultured parenchymal rat hepatocytes. Annexin A3 protein was detected in 48-h, but not 2.5-h, cultured hepatocytes using Western blot analysis. The annexin A3 level further increased after an additional 24 h of culture. Annexin A3 mRNA was not detected in 2.5-h cultured hepatocytes but was detected 22 h after the start of culture by RT-PCR analysis, reaching a maximum value after 48 h of culture. To define the role of Annexin A3 in DNA synthesis, RNA interference was used to reduce annexin III gene expression in hepatocytes. The transfection of small interfering RNAs targeting annexin A3 in the hepatocytes reduced the corresponding mRNA and protein expression by approximately 80% and more than 90%, respectively, at 24 h after transfection. In the annexin A3 small interfering RNAs-transfected cells, DNA synthesis, as assessed by [^{3}H]thymidine incorporation, decreased by approximately 70% not only in the control cultures, but also in the hepatocyte growth factor- or epidermal growth factor-treated cells. These findings show that annexin A3 is expressed in primary cultured parenchymal rat hepatocytes and that the suppression of annexin A3 expression using RNA interference inhibits DNA synthesis.

Key words annexin A3; RNAi; DNA synthesis; primary cultured hepatocyte; hepatocyte growth factor (HGF); epidermal growth factor (EGF)

Annexin (Anx) A3 is also called "lipocortin 3" or "placental anticoagulant protein 3" (PAP-III)[1] and is a member of the lipocortin/annexin family, which binds to phospholipids and membranes in a Ca^{2+}-dependent manner.[2—4] AnxA3 has been shown to have anticoagulant and anti-phospholipase A_2 properties *in vitro*[5] and to promote the Ca^{2+}-dependent aggregation of isolated specific granules from human neutrophils.[6] Although the physiological functions of other annexins have been recently clarified in knock-out and transgenic models,[7—14] the functions of AnxA3 are completely unknown.[15]

Recently, we found that AnxA3 protein and its mRNA are not expressed in isolated parenchymal rat hepatocytes.[16,17] Consistent with these findings, AnxA3 protein and its mRNA are not detectable by Western blot analysis and Northern blot analysis in rat liver.[18—21] However, there have been no reports on the behavior of AnxA3 in primary cultured parenchymal rat hepatocytes. In the present study, we investigated the expression and function of AnxA3 in cultured parenchymal rat hepatocytes.

MATERIALS AND METHODS

Materials Recombinant human hepatocyte growth factor (HGF) was purchased from R&D systems (Minneapolis, MN, U.S.A.). Mouse epidermal growth factor (EGF) was purchased from Wako (Osaka, Japan). [^{3}H]thymidine (79.9 Ci/mmol) was purchased from PerkinElmer (Boston, MA, U.S.A.). Rabbit anti-human ANXA3 antibody serum was a generous gift from Dr. F. Russo-Marie and Dr. C. Raguenness-Nicol.

Cell Isolation and Monolayer Cultures Parenchymal hepatocytes were isolated from adult male Wistar rats, weighing 180—200 g, by *in situ* perfusion of the liver with collagenase.[22] All animal care and procedure protocols were approved by the institutional care committee. The cells were then suspended at a density of 2.5×10^5 cells/ml in Williams E medium (WE) containing 5% fetal bovine serum and 1 nM insulin and cultured at a density of 0.5×10^5 cells/cm^2 in a 6 cm dish and a 48-well microplate precoated with collagen type-I AC in a humidified chamber at 37 °C in 5% CO_2 and 30% O_2 in air. Cells plated in the 6-cm dish and 48-well microplate were used to prepare total cellular extracts or total RNA and to measure DNA synthesis, respectively. After 2.5 h of culture, the medium was replaced with a serum- and hormone-free medium containing aprotinin (1 μg/ml).

Western Blot Analysis Cell lysates were prepared using a modification of a previously described method.[23] The cells were washed with phosphate-buffered saline (PBS) followed by buffer A (50 mM Tris–HCl [pH 7.5], 150 mM NaCl, and 10 mM EDTA). The cells were then harvested after the addition of 20 μl of buffer A. The cells were suspended, shaken for 15 min at room temperature, and sonicated five times for 15 s each time while in an ice bath after the addition of 1/5 [v/v] of 5×buffer A containing 2.5% Triton X-100 and 1/100 [v/v] of a protease inhibitor cocktail (SIGMA). After centrifugation at 100000×g, the cytosolic fraction (about 25 μg) was subjected to sodium dodecyl sulfate-polyacrylamide gel

* To whom correspondence should be addressed. e-mail: niimi@nihs.go.jp

electrophoresis on a 10% gel and electroblotted to a PVDF membrane (GVHP; Millipore). After blocking the membrane with 5% skimmed milk, a Western blot analysis was performed using rabbit anti-human AnxA3 antibody serum at a dilution of 1 : 18000; detection was performed using the ECL detection system (Amersham Bioscience).

Reverse Transcription Polymerase Chain Reaction Analysis Total RNA was exctracted from the cells using Trizol reagent (Invitrogen) according to the manufacturer's protocols. Approximately 3 μg of RNA per sample was reverse-transcribed using the THERMOSCRIPT™ RT-PCR System (Invitrogen) and oligo$(dT)_{20}$ in a final volume of 40 μl, according to the manufacturer's protocols. Subsequently, 1 μl of cDNA was polymerase chain reaction (PCR)-amplified using the THERMOSCRIPT™ RT-PCR System (Invitrogen) in a final volume of 20 μl per reaction, according to the manufacturer's protocols, for 14—23 cycles of denaturation for 30 s at 94 °C, annealing for 30 s at 60 °C, and polymerization for 1 min at 72 °C using Anx AIII or glyceraldehyde 3-phosphate dehydrogenase (GAPDH) cDNA specific primers under linear conditions. The PCR products were separated on a 2% agarose gel, stained with SYBR Green I, and visualized and analyzed with a FluorolImager 595 (Amersham Bioscience). A computer assisted-analyzer was used to quantitatively analyze the signals, and the signals were normalized to the signal of a house keeping gene, the gene coding GAPDH. The sequences of the AnxA3 primers were as follows: 5′-CAAATTCACCGAGATCCTGT-3′ and 5′-TGCTGGAGTGCTGTACGAAA-3′. The sequences of the GAPDH primers were as follows: 5′-ACCACAGTCCATGCCATCAC-3′ and 5′-TCCACCACCTGTTGCTGTA-3′.[24] The PCR product specificity was confirmed by DNA sequence analysis using an ABI Prism 377 DNA Sequencer (Applied Biosystems, Foster City, CA, U.S.A.).

Preparation and Transfection of Small Interfering RNAs Targeting AnxA3 Small interfering RNAs (siRNAs) targeting rat AnxA3 were designed according to the guidelines of the "Dharmacon siDESIGN Center" (www.dharmacon.com) and obtained from Dharmacon Research (Lafayette) in annealed and lyophilized forms. The target sequences were localized at positions, 493 and 690 bps downstream of the start codon. The sequences of each siRNA pair were as follows: AnxA3 siRNA 1, 5′-GAG ACG AAA GCC UGA AAG UdTdT-3′ and ACU UUC AGG CUU UCG UCU cdTdT-3′; ANXA3 siRNA 2, 5′-GGA GAA UUA UCU GGG CAU UdTdT-3′ and AAU GCC CAG AUA AUUCUC cdTdT-3; and control siRNA, 5′-ACU CUA UCU GCA CGC UGA CUU-3′ and 5′-P G UCA GCG UGC AGA UAG AGU UU-3′. No homology between any relevant mammalian gene and the control siRNA was observed. These siRNAs were dissolved in an RNase-free solution provided by Dharmacon Research at a concentration of 20 μM. After 20 h of cell culture, the medium was replaced with WE containing aprotinin (1 μg/ml) immediately prior to transfection. Transfection with siRNA was performed using SiFector (B-bridge), according to the user guidelines. Sixty microliters of both AnxA3 siRNA 1 and 2 were diluted with OPTI-MEM (Invitrogen) to a final volume of 400 μl. Sixty-four microliters of SiFector was also diluted in OPTI-MEM to a final volume of 400 μl, then suspended and incubated at room temperature for 5 min. Next, the diluted siRNA was combined with SiFector, and the mixture was incubated at room temperature to allow the siRNA-SiFector complex to form. Eight hundred microliters of the siRNA-SiFector complex was added to the cultures (6-cm dish). For the 48-well plates, the siRNA-SiFector complex was prepared as described above except that the volume of each solution per well was scaled down to 1/16.

Measurement of [^{3}H]thymidine Incorporation After 20 h of culture, the medium was replaced with hormone-free medium containing aprotinin (1 μg/ml) and 0.1% bovine serum albumin (BSA), and EGF (2 ng/ml) or HGF (20 ng/ml) was added. After 1 h, 50 μl of siRNA-SiFector complex, prepared as described above, was added to the wells. After another 24 h, [^{3}H]thymidine (0.626 μCi) and thymidine (676.6 ng) were added, and 10 μg/ml of aphidicolin was added to some wells at the same time. The cells were then cultured for another 24 h. [^{3}H]thymidine incorporation was measured as described previously.[25] The difference between the radioactivity in the hot-trichloroacetic acid soluble fraction with and without aphidicolin was calculated as dpm/mg protein. Cell protein was measured using a previously described method,[26] with BSA used as a standard.

RESULTS

Expression of AnxA3 during Culture At first, we investigated the expression of AnxA3 in primary cultured parenchymal rat hepatocytes. AnxA3 protein was not detected by Western blot analysis 2.5 and 24 h after the start of culture but was detected after 48 h of culture (Fig. 1A). The level after 72 h of culture was approximately 1.6-fold higher than that after 48 h of culture (Fig. 1B). AnxA3 mRNA was not detected by reverse transcription (RT)-PCR in cultured hepatocytes after 2.5 h of culture but was significantly detected after 22 h of culture (Fig. 2A), reaching a maximum value after 48 h of culture (Fig. 2B). These results indicate

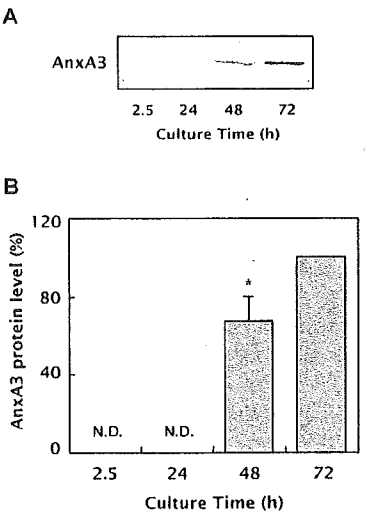

Fig. 1. Expression of AnxA3 Protein during Culture

(A) The data shown are representative of the Western blot analysis results. Cells lysates were prepared from the cells at the indicated times and used for the Western blot analysis. (B) The intensity of each band was quantified, and the results are shown relative to the value of cells cultured for 72 h. The data are expressed as the mean±S.D. of 3 experiments. *$p<0.01$, compared with the value of cells cultured for 72 h. N.D., not detected.

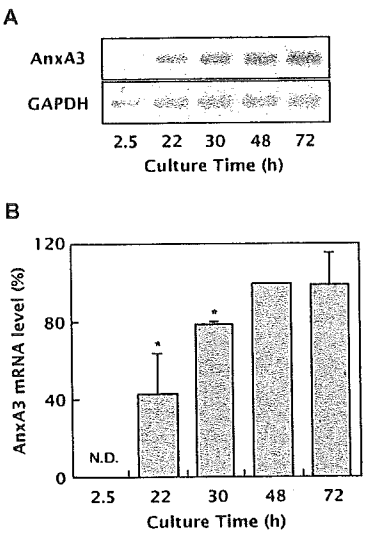

Fig. 2. Increase in AnxA3 mRNA Level during Culture

(A) The data shown are representative of the RT-PCR analysis results. Total RNA was prepared from the cells at the indicated times and used for the RT-PCR analysis. (B) The intensity of each band was quantified, and the results are shown relative to the value of cells cultured for 48 h. The data are expressed as the mean±S.D. of 3 experiments. *$p<0.01$, compared with the value of cells cultured for 48 h. N.D., not detected.

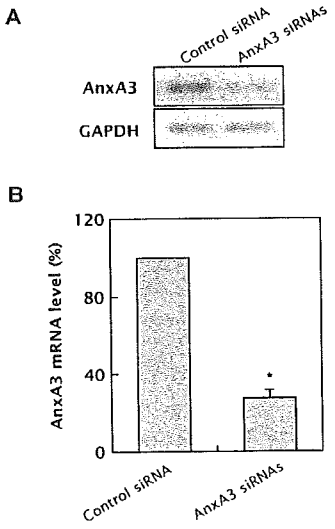

Fig. 3. Suppression of Increase in AnxA3 mRNA Level during Culture with RNAi

(A) The data shown are representative of the RT-PCR analysis results. Total RNA was prepared from the cells 1 d after siRNA transfection and used for the RT-PCR analysis. (B) The intensity of each band was quantified, and the results are shown relative to the value of cells transfected with control siRNA. The data are expressed as the mean±S.D. of 3 experiments. *$p<0.01$, compared with the value of cells transfected with control siRNA.

that the expression of AnxA3 is regulated by its mRNA level.

Suppression of AnxA3 Expression Using RNA Interference Next, we attempted to suppress AnxA3 expression by RNA interference (RNAi) to examine the role of ANXA3 in the cultured hepatocytes. AnxA3 mRNA expression was markedly reduced by treatment with AnxA3 siRNAs, compared with the expression after treatment with control siRNA, 1 d after the transfection (Fig. 3A), with an inhibition of approximately 80% (Fig. 3B). Furthermore, the AnxA3

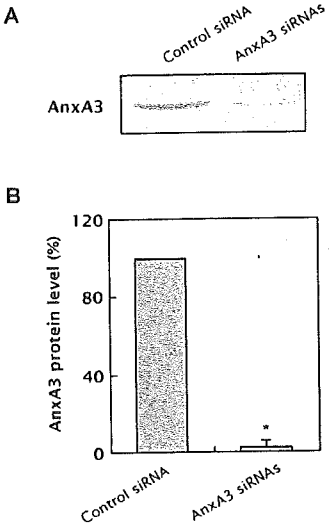

Fig. 4. Suppression of AnxA3 Protein Expression during Culture with RNAi

(A) The data shown are representative of the Western blot analysis results. Cells lysates were prepared from the cells 1 d after siRNA transfection and used for the Western blot analysis. (B) The intensity of each band was quantified, and the results are shown relative to the value of cells transfected with control siRNA. The data are expressed as the mean±S.D. of 3 experiments. *$p<0.01$, compared with the value of cells transfected with control siRNA.

protein level was also reduced by the treatment with AnxA3 siRNAs compared with the level after treatment with control siRNA (Fig. 4A), with an inhibition of more than 95% (Fig. 4B). On the other hand, the control siRNA had almost no effect on AnxA3 protein and mRNA levels compared with those treated with SiFector alone (data not shown). Neither the control nor AnxA3 siRNAs caused any cytotoxic effects, as observed microscopically or by the quantification of the total amount of protein in each sample (data not shown). These results indicate that AnxA3 siRNAs efficiently and specifically, inhibit the expression of AnxA3 in primary cultured parenchymal rat hepatocytes.

Inhibition of DNA Synthesis by Suppression of AnxA3 Expression Using RNAi Finally, we examined the role of AnxA3 in DNA synthesis by suppressing AnxA3 expression using RNAi. EGF (2 ng/ml) and HGF (20 ng/ml) stimulated DNA synthesis by approximately 7-fold and 9-fold, respectively in hepatocytes treated with control siRNA (Fig. 5). The stimulations were inhibited to approximately 70% by treatment with AnxA3 siRNAs. Similar results were also obtained in the control cells, whereas the control siRNA had almost no effect on DNA synthesis, compared with the effect in cells treated with SiFector alone (data not shown).

DISCUSSION

In the present study, we showed for the first time that AnxA3 is expressed in cultured parenchymal rat hepatocytes and that the inhibition of AnxA3 expression by RNAi resulted in a significant inhibition of DNA synthesis, suggesting that the expression of AnxA3 is necessary for DNA synthesis in primary cultured parenchymal rat hepatocytes.

Hepatocytes placed under culture conditions, are known to acquire a growth potential characterized by the enhancement of DNA synthesis, which is caused by several growth

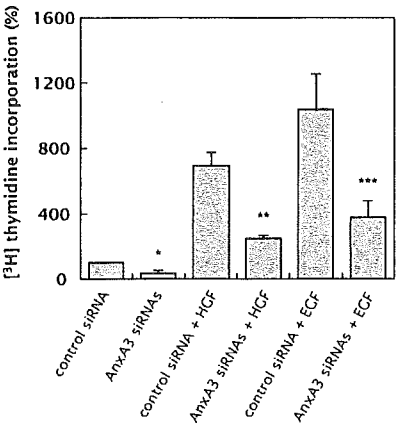

Fig. 5. Inhibition of DNA Synthesis by RNAi

The results are shown relative to the value of control cultured cells transfected with control siRNA. The data are expressed as the mean±S.D. of duplicate wells in 3 experiments. *$p<0.01$, compared with the value of control cultured cells transfected with control siRNA. **$p<0.01$, compared with the value of cells cultured in the presence of HGF and transfected with control siRNA. ***$p<0.01$, compared with the value of cells cultured in the presence of EGF and transfected with control siRNA. The mean±S.D. of [^{3}H]thymidine incorporation in the control cultured cells transfected with control siRNA was $9.72\times10^4\pm0.68\times10^4$ dpm/mg protein.

factors.[27,28] Our present findings suggest that the expression of AnxA3 is partly necessary for hepatocytes to acquire a growth potential under culture conditions. In fact, the enhanced expression of AnxA3 has been observed in hepatocellular carcinoma cell lines.[29] In addition, we discovered that the enhanced expression of Anx3 was observed in the proliferative hepatocytes after carbon tetrachloride-induced rat liver damage (unpublished observations).

As for other annexins, several findings concerning the relation of AnxA1 to hepatocyte growth has been reported as described below. The suppression of AnxA1 expression using antisense technology inhibited proliferation in a mouse hepatocyte cell line.[30] AnxA1 increased in the proliferative hepatocytes after carbon tetrachloride-induced rat liver damage or a partial hepatectomy and in hepatocellullar carcinoma tissue.[31,32]

Although the mechanism of action of AnxA3 on DNA synthesis is presently uncertain, the target of AnxA3 may be a common signal transduction pathway, and not necessarily a constitutive or growth factor-mediated one, because the suppression of AnxA3 expression using RNAi not only inhibited the control of DNA synthesis, but also EGF- or HGF-stimulated DNA synthesis, almost to a similar level. In this respect, the findings described below may be relevant to speculations on the mechanism of action of AnxA3 on DNA synthesis. The growth factor-mediated enhancement of hepatocyte growth consists of several signal transduction pathways.[33] The activation of cytosolic phospholipase A_2 ($cPLA_2$) by MAP kinase liberates arachidonic acid from phospholipids and is followed by the generation of prostaglandins, mediators of DNA synthesis, *via* cyclooxygenase. Interestingly, the suppression of AnxA1 expression using antisense technology inhibited $cPLA_2$ activity in a mouse hepatocyte cell line.[30] This report suggests that $cPLA_2$ must be phosphorylated by AnxA1 to become active. Additional evidence suggests that AnxA1 (275—346 aa), the region responsible for phospholipid binding is necessary for the interaction between AnxA1 and $cPLA_2$.[34] Further study is required to clarify the mechanism of action of AnxA3, including the possibility that AnxA3 positively modulates $cPLA_2$ activity, as in the case of AnxA1.

Acknowledgements This work was supported by grants for Health and Welfare Research from the Japanese Ministry of Health, Labor and Welfare.

REFERENCES

1) Crumpton M. J., Dedman J. R., *Nature* (London), **345**, 212 (1990).
2) Raynal P., Pollard H. B., *Biochim. Biophys. Acta*, **1197**, 63—93 (1994).
3) Gerke V., Moss S. E., *Physiol. Rev.*, **82**, 331—371 (2002).
4) Moss S. E., Morgan R. O., *Genome Biol.*, **5**, 219. 1—8 (2004).
5) Tait J. F., Sakata M., McMullen B. A., Miao C. H., Funakoshi T., Hendrickson L. E., Fujikawa K., *Biochemistry*, **27**, 6268—6276 (1988).
6) Ernst J. D., Hoye E., Blackwood R. A., Jaye D., *J. Clin. Invest.*, **85**, 1065—1071 (1990).
7) Gunteski-Hamblin A. M., Song G., Walsh R. A., Frenzke M., Boivin G. P., Dorn G. W., 2nd, Kaetzel M. A., Horseman N. D., Dedman J. R., *Am. J. Physiol.*, **270**, H1091—1100 (1996).
8) Kubista H., Hawkins T. E., Patel D. R., Haigler H. T., Moss S. E., *Curr. Biol.*, **9**, 1403—1406 (1999).
9) Srivastava M., Atwater I., Glasman M., Leighton X., Goping G., Caohuy H., Miller G., Pichel J., Westphal H., Mears D., Rojas E., Pollard H. B., *Proc. Natl. Acad. Sci. U.S.A.*, **96**, 13783—13788 (1999).
10) Herr C., Smyth N., Ullrich S., Yun F., Sasse P., Hescheler J., Fleischmann B., Lasek K., Brixius K., Schwinger R. H., Fassler R., Schroder R., Noegel A. A., *Mol. Cell. Biol.*, **21**, 4119—4128 (2001).
11) Song G., Harding S. E., Duchen M. R., Tunwell R., O'Gara P., Hawkins T. E., Moss S. E., *Faseb. J.*, **16**, 622—624 (2002).
12) Roviezzo F., Getting S. J., Paul-Clark M. J., Yona S., Gavins F. N., Perretti M., Hannon R., Croxtall J. D., Buckingham J. C., Flower R. J., *J. Physiol. Pharmacol.*, **53**, 541—553 (2002).
13) Hannon R., Croxtall J. D., Getting S. J., Roviezzo F., Yona S., Paul-Clark M. J., Gavins F. N., Perretti M., Morris J. F., Buckingham J. C., Flower R. J., *Faseb. J.*, **17**, 253—255 (2003).
14) Croxtall J. D., Gilroy D. W., Solito E., Choudhury Q., Ward B. J., Buckingham J. C., Flower R. J., *Biochem. J.*, **371**, 927—935 (2003).
15) Rand J. H., *N. Engl. J. Med.*, **340**, 1035—1036 (1999).
16) Niimi S., Hyuga M., Harashima M., Seki T., Ariga T., Kawanishi T., Hayakawa T., *Biol. Pharm. Bull.*, **27**, 1864—1868 (2004).
17) Niimi S., Oshizawa T., Yamaguchi T., Harashima M., Seki T., Ariga T., Kawanishi T., Hayakawa T., *Biochem. Biophys. Res. Commun.*, **300**, 770—774 (2003).
18) Kaetzel M. A., Hazarika P., Dedman J. R., *J. Biol. Chem.*, **264**, 14463—14470 (1989).
19) Comera C., Rothhut B., Cavadore J. C., Vilgrain I., Cochet C., Chambaz E., Russo-Marie F., *J. Cell. Biochem.*, **40**, 361—370 (1989).
20) Kristensen B. I., Kristensen P., Johnsen A. H., *Int. J. Biochem.*, **25**, 1195—1202 (1993).
21) Pepinsky R. B., Tizard R., Mattaliano R. J., Sinclair L. K., Miller G. T., Browning J. L., Chow E. P., Burne C., Huang K. S., Pratt D., Walchter L., Hession C., Frey A. Z., Wallner B. P., *J. Biol. Chem.*, **263**, 10799—10811 (1988).
22) Tanaka K., Sato M., Tomita Y., Ichihara A., *J. Biochem.* (Tokyo), **84**, 937—946 (1978).
23) Romisch J., Schuler E., Bastian B., Burger T., Dunkel F. G., Schwinn A., Hartmann A. A., Paques E. P., *Blood Coagul. Fibrinolysis*, **3**, 11—17 (1992).
24) Uno S., Nakamura M., Seki T., Ariga T., *Biochem. Biophys. Res. Commun.*, **239**, 123—128 (1997).
25) Niimi S., Horikawa M., Seki T., Ariga T., Kobayashi T., Hayakawa T., *Biol. Pharm. Bull.*, **25**, 437—440 (2002).
26) Bradford M. M., *Anal. Biochem.*, **72**, 248—254 (1976).
27) Fausto N., Laird A. D., Webber E. M., *Faseb. J.*, **9**, 1527—1536 (1995).
28) Michalopoulos G. K., DeFrances M. C., *Science*, **276**, 60—66 (1997).
29) Liang R. C., Neo J. C., Lo S. L., Tan G. S., Scow T. K., Chung M. C., *J. Chromatogr. B Analyt. Technol. Biomed. Life Sci.*, **771**, 303—328 (2002).
30) de Coupade C., Gillet R., Bennoun M., Briand P., Russo-Marie F.,

Solito E., *Hepatology*, **31**, 371—380 (2000).
31) Masaki T., Tokuda M., Fujimura T., Ohnishi M., Tai Y., Miyamoto K., Itano T., Matsui H., Watanabe S., Sogawa K., Yamada T., Konishi R., Nishioka M., Hatase O., *Hepatology*, **20**, 425—435 (1994).
32) Masaki T., Tokuda M., Ohnishi M., Watanabe S., Fujimura T., Miyamoto K., Itano T., Matsui H., Arima K., Shirai M., Maeba T., Sogawa K., Konishi R., Taniguchi K., Hatanaka Y., Hatase O., Nishioka M., *Hepatology*, **24**, 72—81 (1996).
33) Adachi T., Nakashima S., Saji S., Nakamura T., Nozawa Y., *Hepatology*, **21**, 1668—1674 (1995).
34) Kim S. W., Rhee H. J., Ko J., Kim Y. J., Kim H. G., Yang J. M., Choi E. C., Na D. S., *J. Biol. Chem.*, **276**, 15712—15719 (2001).

J Pharmacol Sci 97, 361 – 368 (2005)

Journal of Pharmacological Sciences

Full Paper

Simultaneous Real-Time Detection of Initiator- and Effector-Caspase Activation by Double Fluorescence Resonance Energy Transfer Analysis

Hiroshi Kawai[1], Takuo Suzuki[1], Tetsu Kobayashi[1], Haruna Sakurai[2], Hisayuki Ohata[2], Kazuo Honda[2], Kazutaka Momose[2], Iyuki Namekata[3], Hikaru Tanaka[3], Koki Shigenobu[3], Ryu Nakamura[4], Takao Hayakawa[1], and Toru Kawanishi[1,*]

[1]*Division of Biological Chemistry and Biologicals, National Institute of Health Sciences, Tokyo 158-8501, Japan*
[2]*Department of Pharmacology, School of Pharmaceutical Sciences, Showa University, Tokyo 142-8555, Japan*
[3]*Department of Pharmacology, Toho University School of Pharmaceutical Sciences, Chiba 274-8510, Japan*
[4]*Carl Zeiss Co., Ltd., Tokyo 160-0003, Japan*

Received August 31, 2004; Accepted January 8, 2005

Abstract. Fluorescence resonance energy transfer (FRET) with green fluorescent protein (GFP) variants has become widely used for biochemical research. In order to expand the choice of fluorescent range in FRET analysis, we designed various color versions of the FRET-based probes for caspase activity, in which the substrate sequence of the caspase was sandwiched by donor and acceptor fluorescent proteins, and studied the potential of these color versions as fluorescent indicators. Six color versions were constructed by a combination of cyan fluorescent protein (CFP), GFP, yellow fluorescent protein (YFP), and DsRed. Real-time monitoring in single cells revealed that all probes could detect caspase activation during tumor necrosis factor (TNF)-α-induced cell death as a fluorescent change. GFP-DsRed and YFP-DsRed were as sensitive as CFP-YFP, and CFP-DsRed also showed a large fluorescent change. By using two probes, CFP-DsRed and YFP-DsRed, we carried out simultaneous multi-FRET analysis and revealed that the initiator- and effector-caspases were activated almost simultaneously in TNF-α-induced cell death. These findings may give experimental bases for the development of novel techniques to analyze multi-events simultaneously in single cells by using FRET probes in combination.

Keywords: fluorescence resonance energy transfer, green fluorescent protein, tumor necrosis factor-α, cell death, caspase

Introduction

Many probes for various physiological reactions have been developed with green fluorescent protein (GFP) variants by using a similar strategy as that used with cameleon, the Ca^{2+}-sensing fusion protein developed by Miyawaki et al. (1 – 9). The cameleon consists of cyan fluorescent protein (CFP), calmodulin, M13 peptide, and yellow fluorescent protein (YFP). This fusion protein senses Ca^{2+} as the change of fluorescence resonance energy transfer (FRET) efficiency between CFP and YFP. Calmodulin binds M13 in the presence of Ca^{2+}, which causes conformational change in cameleon, resulting in a change in the distance between and relative orientation of CFP and YFP. This change alters the FRET efficiency from CFP to YFP; therefore, Ca^{2+} can be monitored as the fluorescent change (1).

CFP and YFP are the most frequently used pair for analysis by FRET. This pair is suitable for FRET analysis because the spectral overlap between the emission of the donor protein (CFP) and the excitation of the acceptor protein (YFP) is sufficient for energy transfer, and their ranges of fluorescence are far apart enough to be separated by measuring devices such as fluorescent microscopy (10). However, there are limitations for the CFP-YFP pair. It is impossible, for example, to use the CFP-YFP FRET probe for simultaneous measurement with other probes that are made of GFP variants or have

*Corresponding author. FAX: +81-3-3700-9064
E-mail: kawanish@nihs.go.jp.

fluorescein structure. If more choice of FRET probes is available from wider fluorescence ranges, it would allow us to analyze multi-events simultaneously occurring in living cells.

In this paper, we developed caspase-sensors of various colors by using cyan, green, yellow, and red fluorescent proteins and assessed their ability to detect the caspase activation in living single cells. Based on the findings obtained, we tried to perform multi-event FRET analysis and clarify the temporal relationships between biochemical reactions during cell death.

Materials and Methods

Plasmid construction

Plasmid encoding CY-sensor, YFP-peptide-CFP, was generated as previously reported (11). The sequence encoding 11 amino acids at the C-terminus of YFP was eliminated in this construct. The C-terminal truncated forms of the CFP (or GFP) gene were generated by PCR with primers containing the NheI site or BspEI site and pECFP-C1 (or pEGFP-C1; Clontech, Palo Alto, CA, USA) as a template, and the restricted fragment was inserted into the NheI/BspEI sites of the CY-sensor to generate a plasmid carrying truncated CFP (or GFP) at the N-terminus. DsRed was generated from pDsRed2-C1 (Clontech) by PCR, at the AgeI/NotI sites, and the restricted fragment was inserted into the AgeI/NotI sites of the CY-sensor to generate a plasmid carrying DsRed2 at the C-terminus. CG-, CR-, GR-, and YR-sensors were generated with a combination of these elements. The AgeI/BsrGI fragment from pEGFP-C1 was inserted into the AgeI/BsrGI sites of the CY-sensor to generate the GY-sensor. All cloned sequences were verified by sequencing.

Cell culture and transfection

HeLa cells were cultured in DMEM (Sigma-Aldrich, St. Louis, MO, USA) supplemented with 100 units/ml of penicillin G, 100 μg/ml of streptomycin, and 10% fetal calf serum (Invitrogen Corp., Carlsbad, CA, USA). Plasmid encoding the sensor protein was transfected into HeLa cells using Effectene Transfection Reagent (Qiagen, Hilden, Germany) according to the manufacturer's instructions. After 12 – 24 h incubation with the transfection reagent, the cells were washed with PBS and cultivated on dishes suitable for assay in medium containing 500 μg/ml of G418 for an additional 1 – 3 days until the assay was performed.

Western blotting

Cells cultured in a plastic dish were washed with PBS and lysed with 1 × SDS loading buffer. The samples dissolved in 1 × SDS loading buffer were incubated at 95°C for 2 min, and then they were loaded onto SDS-polyacrylamide gels (10%). Proteins were separated at 20 mA and then blotted to PVDF membranes in Tris-glycine transfer buffer at 100 V for 2 h. The membrane was incubated with block ace (Dainippon Pharmaceutical, Osaka) for 1 h, anti-GFP peptide antibody (Clontech, diluted with 0.1 × block ace to 1:1,000) for 2 h, and anti-rabbit IgG horseradish peroxidase-conjugated secondary antibody (Chemicon International Inc., Temecula, CA, USA; diluted with 0.1 × block ace to 1:10,000) for 1 h. The membrane was washed with TBS-T 3 times for 5 min after the incubation with the antibody. All of these incubations were performed at room temperature. The membrane was developed with the ECL chemiluminescence detection reagent (Amersham Biosciences, Piscataway, NJ, USA).

Measurement of fluorescent spectra of the sensors in HeLa cells

Spectral imaging was performed with LSM510META (Carl Zeiss, Jena, Germany) (12). Cells expressing one of the sensors were observed by excitation light at 458 nm (Ar laser), emitted fluorescence was separated by a grating, and the separated fluorescence were detected by 24 photomultiplier tubes (PMT) that were set to detect fluorescence at 468 – 714 nm. Each PMT detected fluorescence in the 10.7-nm wavelength range. So, the fluorescent spectrum at 468 – 714 nm was obtained with 10.7-nm resolution. Cell death was induced by incubation with tumor necrosis factor (TNF)-α (100 ng/ml) and cycloheximide (CHX, 10 μg/ml) for 6 h. Fluorescent spectra of living and dead cells were obtained from the whole cell region of normal-shaped and spherical cells, respectively.

Real-time imaging with FRET sensors

Transfected cells were cultured on a cover glass (25-mm diameter, 0.15 – 0.18-mm thickness) for 1 – 3 days. Cells were treated with TNF-α/CHX and then incubated under the usual culture condition for 1 – 2 h before analysis. Analyses were carried out by confocal laser-scanning fluorescent microscopy using a Carl Zeiss LSM510 system. During the observation, the media were buffered with 10 mM hepes buffer (pH 7.4), and the cells were maintained at 35 – 37°C. DIC images and grayscale images for fluorescence channels were obtained every 2 min unless otherwise described. Excitation lights for the FRET probe (458 nm for the CG-, CY-, GY-, and CR-sensors; 488 nm for the GR- and YR-sensors) were provided by an Ar laser with a 458 or 488 dichroic mirror. Images of the FRET probe were obtained separately for both donor and acceptor

Table 1. Measurement conditions for real-time analysis by LSM510

Sensor	Fusion protein[a]	Excitation (nm)[b]	Emission (nm)[c]		
			beam splitter	emission filter	
				donor	acceptor
CG	GFP-peptide-CFP	458	515	467.5 – 497.5	515 – 545
CY	YFP-peptide-CFP	458	515	467.5 – 497.5	515 – 545
GY	YFP-peptide-GFP	458	515	475 – 525	515 – 545
CR	CFP-peptide-DsRed	458	515	467.5 – 497.5	560 – 615
GR	GFP-peptide-DsRed	488	545	505 – 530	560 – 615
YR	YFP-peptide-DsRed	488	545	505 – 530	560 – 615

[a]N-terminal CFP, GFP, and YFP were in a truncated form in which 11 amino acids at the C-terminus were eliminated, and His_{10} was present at the C-terminus of CG, CY, and GY. [b]Excitation light was obtained by Ar laser and a 458 or 488 dichroic mirror. [c]Emitted fluorescence was separated by a 515 or 545 dichroic mirror, and the fluorescence of the donor and that of the acceptor were obtained through band pass emission filters.

fluorescence using a dichroic mirror and band-pass emission filters as shown in Table 1. Images were processed and quantified using MetaFluor software as follows: The average pixel intensity of the fluorescence of the whole cell region was determined for each channel. The ratio value was calculated as the average pixel value of the fluorescent ratio, (fluorescent intensity for the acceptor channel) / (fluorescent intensity for the donor channel), in the whole cell region. As cells changed their morphology during the observation, the whole cell region was determined separately in each image.

Results

Construction and characterization of FRET probes

We developed plasmids expressing caspase sensors as shown in Fig. 1a. A 12-amino-acid peptide derived from poly(ADP-ribose)polymerase (PARP) that is a well-known substrate of effector caspases was sandwiched by two different fluorescent proteins (an example of CFP-YFP is shown in Fig. 1a). The peptide sequence contains a caspase recognition site in the middle, and this fusion protein was cleaved mainly by caspase-3 (11). CFP-GFP, CFP-YFP, GFP-YFP, CFP-DsRed, GFP-DsRed, and YFP-DsRed were used as the donor-acceptor pairs. We named these fusion proteins CG-, CY-, GY-, CR-, GR-, and YR-sensor, respectively (Table 1). These fusion proteins show FRET in their intact form, whereas in the presence of active caspase, the peptide sequence is cleaved, CFP and YFP are far apart, and the fusion proteins do not show FRET any longer. The fluorescent ratio of acceptor/donor reflects the amount of FRET, so we used the reduction of this value as an index of caspase activation.

HeLa cells expressing one of these fusion proteins

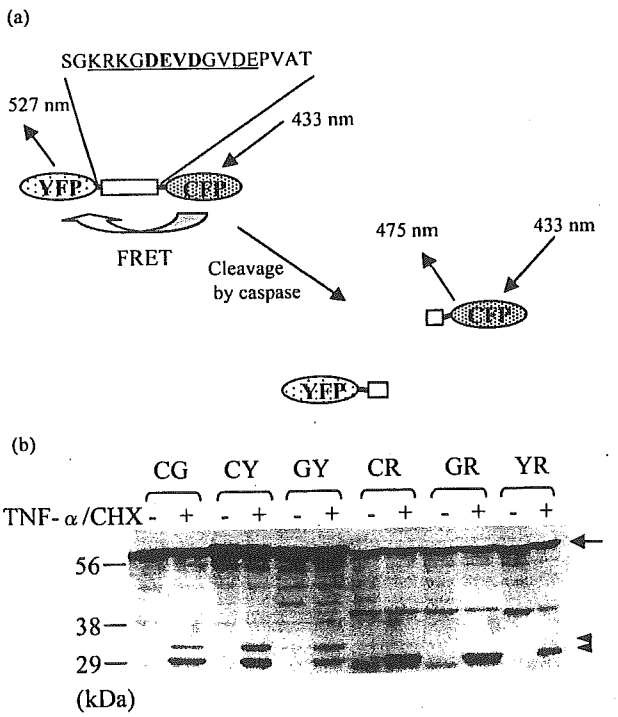

Fig. 1. Small peptide sandwiched by two different fluorescent proteins can be a caspase-sensor. a: Fusion protein that consists of a PARP-derived 12-amino-acid peptide sandwiched by CFP and YFP exhibits FRET in its intact form. In the presence of active caspases, the peptide is cleaved, and the fusion protein does not exhibit FRET. Caspase activation can be detected by measuring the fluorescence of CFP and YFP. b: Six caspase-sensors expressed in HeLa cells were cleaved by cell death stimuli. HeLa cells expressing one of the sensors were incubated in the presence or absence of TNF-α/CHX for 6 h. The arrow and arrowhead indicate the full length and cleaved fragments of the sensors.

were treated with TNF-α/CHX. After 6-h exposure, the sensor proteins in cells were extracted and analyzed by western blotting. All 6 fusion proteins were detected in their intact forms in non-treated HeLa cells (arrow in Fig. 1b), and small fragments were detected in cells treated with TNF-α/CHX (arrowhead in Fig. 1b), indicating that the fusion proteins were cleaved by cell death stimuli, as expected. The antibody used in this analysis reacts with CFP, GFP, and YFP, but not with DsRed. Therefore, CG-, CY-, and GY-sensor showed two cleaved fragments corresponding to the N- and C-terminal C/G/YFP, whereas CR-, GR-, and YR-sensor showed only one cleaved fragment corresponding to the N-terminal C/G/YFP.

Figure 2 shows the fluorescent spectra of the probes in living or dead cells. Comparing the fluorescence of living and dead cells, all sensors showed an increase of donor fluorescence and/or a reduction of acceptor fluorescence in response to cell death stimuli. This change results in a reduction of fluorescent ratio of acceptor/donor that is an index of FRET. These sensors were designed to show a reduction of FRET with caspase activation, so these results suggest that all 6 fusion proteins work as expected and can detect caspase activation as fluorescent change in living cells.

For simultaneous application of two or more fluorescent probes, minimum spectral overlap between probes is one of the important conditions. The spectra in Fig. 2 give us a clue to determine a suitable combination of probes for multi-probe analysis. CG-, CY-, or GY-sensor has the least fluorescence in the red-fluorescence region (>600 nm), so it is possible to use this fluorescent region for another dye. We can use a red-fluorescent dye that has fluorescence in this region together with CG-, CY-, or GY-sensor simultaneously. On the other hand, YR-sensor has the least fluorescence in the blue-cyan region (<500 nm), so blue-cyan-fluorescent dye is applicable with this probe for the purpose of simultaneous fluorescence imaging. The color variations of FRET probe may be useful for multi-probe analysis.

Real-time detection of caspase activation in living cells

Next, we applied the sensor proteins to real-time measurement. HeLa cells expressing one of the sensor proteins were analyzed with a time resolution of 2 min by laser-scanning confocal fluorescent microscopy. Figure 3 shows typical images (a) and fluorescent changes (b) during cell death. HeLa cells expressing GR-sensor were treated with TNF-α/CHX. An increase of donor protein fluorescence (GFP), a reduction of acceptor protein fluorescence (DsRed), and a reduction of the fluorescent ratio of acceptor/donor (DsRed/GFP) were observed in each cell at a different time. Caspases began to work at the point when the fluorescent ratio began to decrease.

All sensors showed similar changes, meaning that all sensors were useful for real-time detection of the caspase activation in a living cell, although the apparent sensitivity was different between sensors. In order to compare the sensitivity of these sensors to detect the caspase activation, the amount of the fluorescent change was calculated. We defined the start point and the end

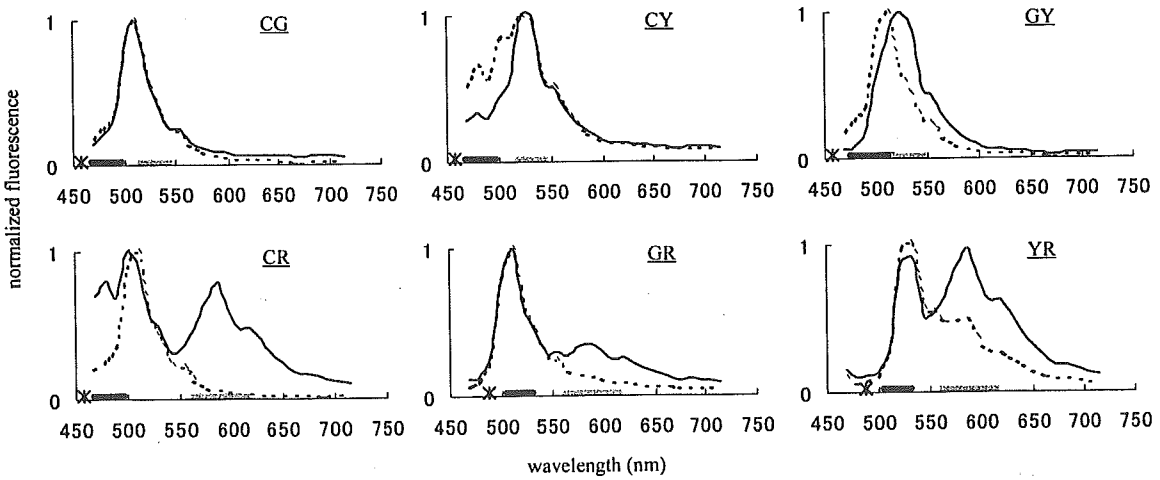

Fig. 2. Fluorescent spectra of the caspase-sensors in HeLa cells. HeLa cells expressing each sensor were treated with TNF-α/CHX for 6 h. The spectra of living cells (solid line) and dead cells (dotted line) were obtained from normal-shaped and spherical cells, respectively. Each spectrum was normalized to the peak that showed maximal intensity. The asterisks and bars on horizontal axes represent the excitation wavelength and detection range for the emitted fluorescence, respectively, used in real-time imaging analysis. Each spectrum is the average of data from 13 – 26 cells.

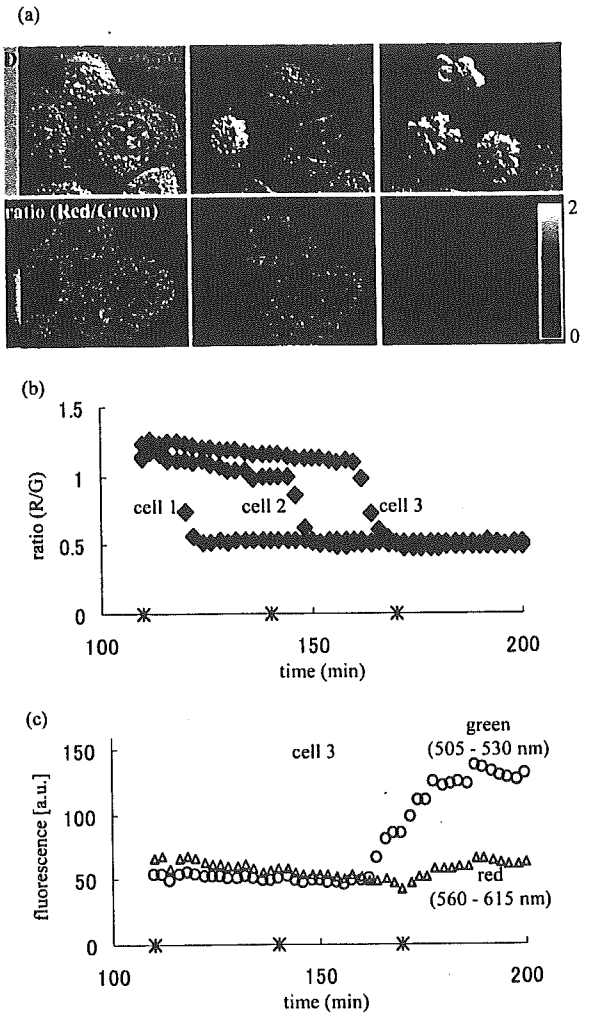

Fig. 3. Real-time imaging of caspase activation in living HeLa cells during cell death. HeLa cells expressing GR-sensor were treated with TNF-α/CHX, and fluorescent images were obtained every 2 min. a: DIC images (upper panels) and fluorescent ratios (Red/Green, lower panels) are shown in grayscale. The indicated time represents the time after the addition of TNF-α/CHX. Scale bar, 10 μm. b: The fluorescent ratio of cells were plotted. Cell 1, 2, or 3 corresponds to the cells shown in panel a. c: The mean pixel intensity in arbitrary fluorescent units (a.u.) for each channel was plotted. The fluorescence of cell No. 3 from panel a is shown. Open circle, GFP; open triangle, DsRed; closed diamond, ratio of Red/Green. Asterisks on the x-axis indicate the time points of the images in panel a.

point of the reduction of the fluorescent ratio as follows: the start point was the point after which the value decreased over four continuous points or more, the value decreased more than 10% in total, and the reduction of the value was not because of artificial noise such as focus shift; the end point followed the start point and was the point at which the value stopped decreasing. The sensitivity of the probe was calculated as $\Delta R = |(R_{end} - R_{start}) / R_{start}|$, where R_{start} and R_{end} were the fluorescent ratio at the start point and the end point, respectively. Figure 4 shows ΔR for each probe. GR and YR, as well as CY, showed the highest ΔR. They each showed a more than 50% change during cell death. CR showed a slightly lower ΔR, but its change was still 44% on average. CG and GY were less sensitive, probably because the fluorescent spectra of the donor and the acceptor were so similar that our system could not effectively measure FRET between them. CY *vs* GR, CY *vs* YR, or GR *vs* YR were not significantly different, and any other comparisons were significantly different by the Games-Howell test ($P<0.05$).

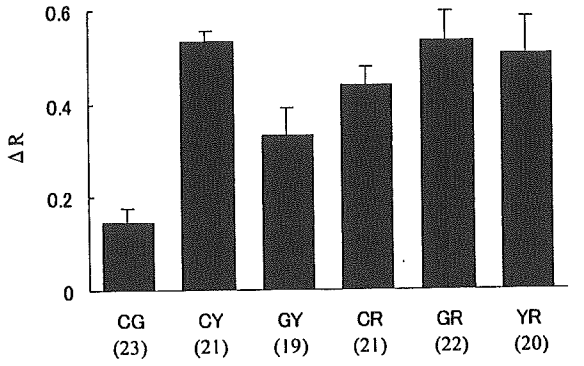

Fig. 4. Comparison of the sensitivity of various caspase-sensors. The amount of change of the fluorescent ratio during cell death (ΔR) was determined in each cell as described in the text. Bars represent means ± S.D. The number of cells used in each analysis is shown in parentheses.

Simultaneous multi-event analysis using two FRET probes

Finally, we tried to perform multi-FRET measurement. We constructed a YR-initiator caspase sensor and a CR-effector caspase sensor by changing the caspase substrate sequence in the sensor and applied them to real-time imaging analysis simultaneously in order to reveal the temporal relationships between the initiator caspase activation and the effector caspase activation in the same cell. The caspase substrate sequences were derived from procaspase-3 and PARP, respectively, and their sequences are shown in Fig. 5a. These sensors were cleaved mainly by caspase-8/9 and caspase-3, respectively (11).

Simultaneous measurement of these sensors was performed under the multi-track scanning mode, in which two sets of excitation-detection conditions were used alternatively. CFP fluorescence by excitation at 458 nm was measured in the first track, and YFP and DsRed fluorescence by excitation at 488 nm was mea-

(a) YFP-SGLDCGIETDSGVDEPVAT-DsRed : YR-(IC)sensor
CFP-SGKRKGDEVDGVDEPVAT-DsRed : CR-(EC)sensor

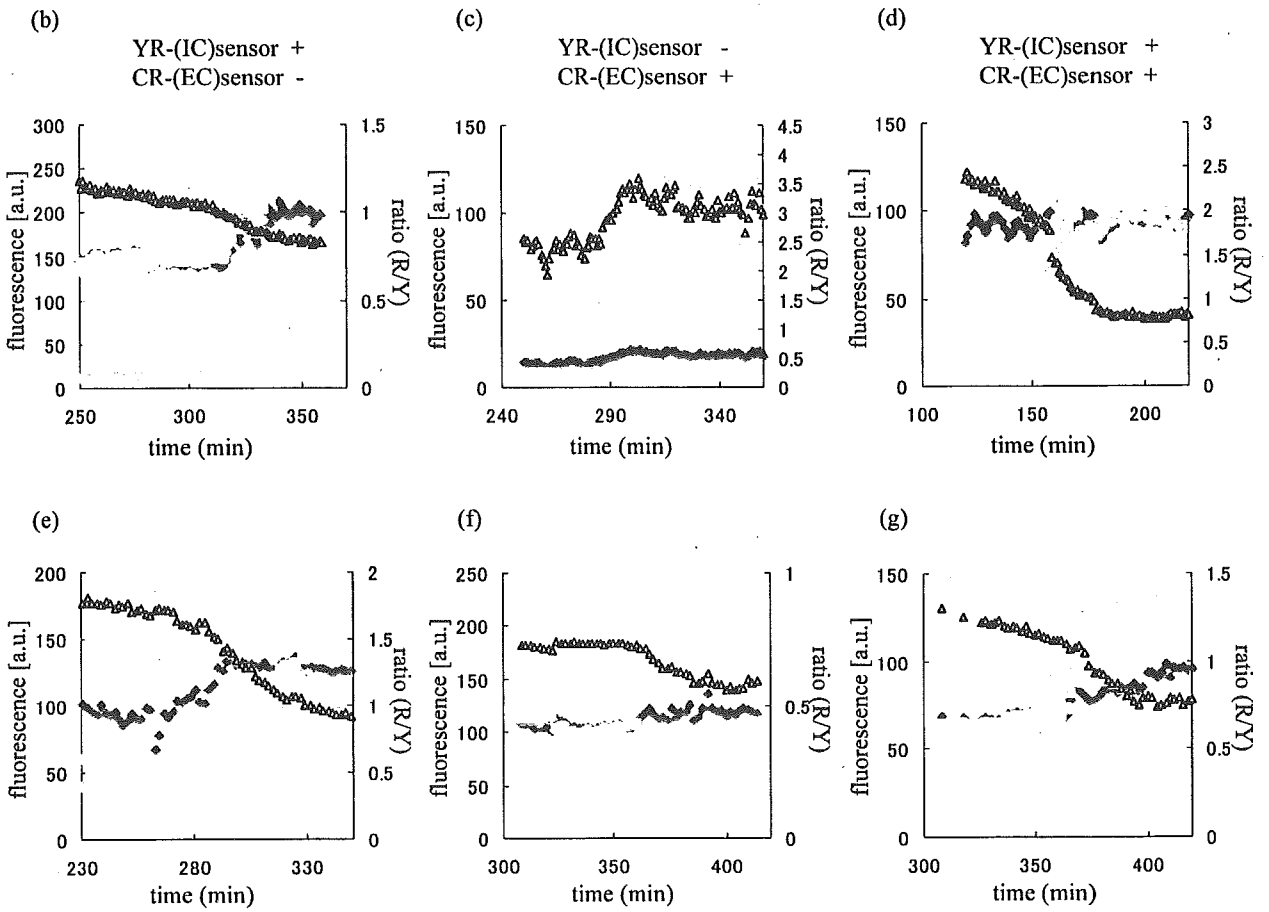

Fig. 5. Simultaneous measurement of initiator- and effector-caspase activation with YR-sensor and CR-sensor. HeLa cells expressing YR-initiator caspase sensor and/or CR-effector caspase sensor were treated with TNF-α/CHX and observed as described in the text. a: Probes used in this study. Underline indicates peptide derived from procaspase-3 and PARP, and bold indicates the consensus 4 amino acid sequence for caspase recognition. b – g: Cells expressing YR-initiator caspase sensor (b), CR-effector caspase sensor (c), or both of them (d – g) were treated with TNF-α/CHX. The fluorescence of CFP, YFP, and DsRed (colored plots) and the fluorescent ratio of DsRed/YFP (open triangles) were plotted against time after TNF-α/CHX treatment.

sured in the second track. The time difference of scanning between tracks is about 3 – 8 s. Figures 5b and 5c show control studies with cells expressing only one of the probes. These control studies were conducted in the same conditions as Fig. 5d. Figures 5b and 5c indicate that the YR- and CR-sensor could detect initiator- and effector-caspase activation as an increase of YFP and CFP signal, respectively, and the contamination of the signal between the YFP and CFP channels was negligible. So, we used an increase of the YFP and CFP signal as index of the initiator- and the effector-caspase activation, respectively. The DsRed signal in Fig. 5c was derived from direct excitation of DsRed in the CR-sensor by the excitation light at 488 nm and was increased when the cell shrank because fluorescent proteins were concentrated in the cell.

Figure 5d shows typical data of multi-probe analysis with the YR-initiator caspase sensor and CR-effector caspase sensor. In this cell, the fluorescence was dramatically changed at 150 – 160 min after TNF-α /CHX treatment. The YFP and CFP signal began to increase almost simultaneously, suggesting that initiator caspase and effector caspase were initially activated within a short time period. Figures 5e – 5g show three

other examples. We observed more than 30 cells in at least 3 independent experiments and found that all dying cells showed similar results.

Discussion

In this study, we developed various color versions of caspase-sensors with CFP, GFP, YFP, and DsRed and revealed that various combinations are applicable in FRET analysis. CY, CR, GR, and YR pairs are preferable FRET pairs that possess a high ability to detect the caspase activation.

The sensitivity shown in Fig. 4 represents the apparent FRET change that depends on the measuring system and was determined by three factors. 1) Intrinsic FRET efficiency: All 4 fluorescent proteins had different fluorescent characteristics; therefore, the levels of FRET efficiency in 6 probes differed from each other. 2) Excitation crosstalk: The acceptors were excited directly by the excitation light. 3) Emission crosstalk: The acceptor channel was contaminated with the donor signal, and vice versa, because the setting shown in Table 1 could not perfectly separate the signals from the donor and the acceptor. The differences in these factors cause the difference of sensitivity among the sensors. Factors 2) and 3) reduce the apparent FRET change in the measurement. In the case of the CG-sensor, for example, fluorescent spectrum of donor and acceptor are so similar that the intrinsic FRET efficiency may be high, but excitation and emission crosstalk may also be high, much higher than in other sensors (e.g., CY-sensor), resulting in the relatively low sensitivity of this probe in our measurement system. Crosstalk effects are undesirable for detection, but it is impossible to completely eliminate these effects in the current measurement system. Maybe we could obtain different results by using spectral imaging in which emission crosstalk is eliminated (12).

According to the characteristics of the fluorescence spectrum, the CY probe seems to be one of the best for FRET-detection. However, the probe is not suitable for imaging with confocal laser microscopy, because the normal argon ion laser, the most common one in confocal microscopes, is not suitable for the excitation of CFP. The blue laser is the most suitable for the excitation, but it is not common in confocal laser microscopes. In this paper, we had to use the argon ion laser emitting 458 nm and the special emission filters optimized for the confocal ratio-imagings of caspase activation using the CY probe (11). On the contrary, the GR probe and the YR probe can be efficiently excited at 488 nm emitted by the normal argon ion laser and imaged with a set of emission filters for fluorescein and a set for rhodamine, with which almost all of the confocal microscopes are equipped. In addition, the GR probe is useful for the detection of caspase activation in flow cytometry, because almost all of the normal flow cytometers are also usually equipped with the laser and the emission filters.

DsRed-containing "red"-sensors have several characteristics that are different from other "non red"-sensors. As previously reported (13), it takes longer for DsRed to mature and emit red fluorescence than it takes for GFPs, and DsRed fluorescence tends to decrease during real-time observation, which may cause a reduction of the apparent sensitivity. These characteristics must be considered when any analysis is performed with these sensors, but as shown in Figs. 4 and 5, red-sensors have a potential similar to that of the CY-sensor and are very useful for multi-color imaging.

It has been reported that DsRed is useful as a fusion tag and a partner for FRET (13, 14). Erickson et al. analyzed the potential of DsRed as a FRET partner with CFP and GFP (14). Mizuno et al. developed a Ca^{2+} sensing fusion protein using Sapphire and DsRed (13). And recently, Karasawa et al. used two novel fluorescent proteins, namely the cyan-emitted and orange-emitted fluorescent proteins from *Acropara* sp. and *Fungia concinna*, respectively, as a FRET pair, and measured caspase-3 activity in cells (15). These results combined with our results indicate that various fluorescent proteins including GFP derivatives, DsRed, and others are useful for FRET analysis. By choosing the appropriate two fluorescent proteins as the FRET pair, we can customize the fluorescent range of FRET-based imaging probes to fit the analysis, which would expand the flexibility of simultaneous multi-event analysis.

By using the CR and YR developed in this study, we were able to analyze two FRET probes simultaneously in the same cells. In several reports, the initiator caspase activity and the effector caspase activity were measured in living cells (8, 9, 11). In these reports, however, each activity was measured independently in different cells. To our knowledge, the present study is the first report that analyzes these activities in the same cell. The results directly reveal the temporal relationships between these caspase activities. It takes a long time for cells to start the initiator caspase activation after drug treatment, but it takes a relatively short time for cells to start the effector caspase activation after the initiator caspase activation. The caspase cascade is initiated at the last stage of cell death signaling, and it proceeds within a short time period.

Acknowledgments

This study was supported in part by a Grant-in-Aid for

Research on Health Sciences Focusing on Drug Innovation from the Japan Health Science Foundation; a Grant-in-Aid for Research on Advanced Medical Technology from the Ministry of Health, Labour, and Welfare; and a grant (MF-16) from the Organization for Pharmaceutical Safety and Research.

References

1 Miyawaki A, Llopis J, Heim R, Mccaffery JM, Adams JA, Ikura M, et al. Fluorescent indicators for Ca^{2+} based on green fluorescent proteins and calmodulin. Nature. 1997;388:882–887.
2 Zaccolo M, Giorgi FD, Cho CY, Feng L, Knapp T, Negulescu PA, et al. A genetically encoded, fluorescent indicator for cyclic AMP in living cells. Nat Cell Biol. 2000;2:25–29.
3 Nagai Y, Miyazaki M, Aoki R, Zama T, Inouye S, Hirose K, et al. A fluorescent indicator for visualizing cAMP-induced phosphorylation in vivo. Nat Biotechnol. 2000;18:313–316.
4 Kurokawa K, Mochizuki N, Ohba Y, Mizuno H, Miyawaki A, Matsuda M. A pair of fluorescent resonance energy transfer-based probes for tyrosine phosphorylation of the CrkII adaptor protein in vivo. J Biol Chem. 2001;276:31305–31310.
5 Sato M, Ozawa T, Inukai K, Asano T, Umezawa Y. Fluorescent indicators for imaging protein phosphorylation in single living cells. Nat Biotechnol. 2002;20:287–294.
6 Tyas L, Brophy VA, Pope A, Rivett AJ, Tavare JM. Rapid caspase-3 activation during apoptosis revealed using fluorescence-resonance energy transfer. EMBO Rep. 2000;1:266–270.
7 Rehm M, Dussmann H, Janicke RU, Tavare JM, Kogel D, Prehn JHM. Single-cell fluorescence resonance energy transfer analysis demonstrates that caspase activation during apoptosis is a rapid process: role of caspase-3. J Biol Chem. 2002;277:24506–24514.
8 Luo KQ, Yu VC, Pu Y, Chang DC. Measuring dynamics of caspase-8 activation in a single living HeLa cell during TNFα-induced apoptosis. Biochem Biophys Res Commun. 2003;304:217–222.
9 Takemoto K, Nagai T, Miyawaki A, Miura M. Spatio-temporal activation of caspase revealed by indicator that is insensitive to environmental effects. J Cell Biol. 2003;160:235–243.
10 Tsien RY. The green fluorescent protein. Annu Rev Biochem. 1998;67:509–544.
11 Kawai H, Suzuki T, Kobayashi T, Mizuguchi H, Hayakawa T, Kawanishi T. Simultaneous imaging of initiator/effector caspase activity and mitochondrial membrane potential during cell death in living HeLa cells. Biochim Biophys Acta. 2004;1693:101–110.
12 Zimmermann T, Rietdorf J, Pepperkok R. Spectral imaging and its applications in live cell microscopy. FEBS Lett. 2003;546:87–92.
13 Mizuno H, Sawano A, Eli P, Hama H, Miyawaki A. Red fluorescent protein from Discosoma as a fusion tag and a partner for fluorescence resonance energy transfer. Biochemistry. 2001;40:2502–2510.
14 Erickson MG, Moon DL, Yue DT. DsRed as a potential FRET partner with CFP and GFP. Biophys J. 2003;85:599–611.
15 Karasawa S, Araki T, Nagai T, Mizuno H, Miyawaki A. Cyan-emitting and orange-emitting fluorescent proteins as a donor /acceptor pair for fluorescence resonance energy transfer. Biochem J. 2004;381:307–312.

J. Biochem. **137**, 579–586 (2005)
DOI: 10.1093/jb/mvi070

Thrombomodulin Enhances the Invasive Activity of Mouse Mammary Tumor Cells

Shingo Niimi[1,*], Mizuho Harashima[2], Kazuko Takayama[2], Mayumi Hara[2], Masashi Hyuga[1], Taiichiro Seki[2], Toyohiko Ariga[2], Toru Kawanishi[1] and Takao Hayakawa[3]

[1]Division of Biological Chemistry and Biologicals, National Institute of Health Sciences, Kamiyoga 1-18-1, Setagaya-ku, Tokyo 158-8501; [2]Department of Nutrition and Physiology, Nihon University College of Bioresource Sciences, Kameino, Fujisawa 252-8510; and [3]Deputy Director General, National Institute of Health Sciences, Kamiyoga 1-18-1, Setagaya-ku, Tokyo 158-8501

Received January 31, 2005; accepted February 18, 2005

Thrombomodulin (TM) is a thrombin receptor on the surface of endothelial cells that converts thrombin from a procoagulant to an anticoagulant. Thrombin promotes invasion by various tumor cells, and positive or negative correlations are found between the expression of TM and tumorigenesis in some patients. In this study, we used an invasion assay to investigate the effect of TM on the invasive activity of a mouse mammary tumor cell line, MMT cells, and the effects of TM were compared with those of thrombin as a positive control. In the presence of 1% fetal calf serum (FCS), TM significantly stimulated MMT cell invasion in a dose-dependent manner, resulting in an approximately 3-fold increase at 1–10 pg/ml over the untreated control. Thrombin also caused a similar degree of stimulation at 50 ng/ml. Since thrombin activity was detected in the components of the assay system, an invasion assay was also performed in a thrombin-activity-depleted assay system constructed to eliminate the effect of thrombin activity; TM (10 pg/ml) plus thrombin (1 pg/ml) stimulated invasion by approximately 3.5-fold in this assay system. Hirudin, a specific thrombin inhibitor, inhibited stimulation by TM as well as by thrombin in both the presence and absence of 1% FCS. Investigations of the effects of TM on proliferation, adhesion and chemotaxis to clarify the mechanism of stimulation by TM revealed that TM does not affect proliferation or adhesion in the presence of 1% FCS, but stimulates chemotaxis by approximately 2.3-fold. Similar results were obtained in experiments using thrombin. TM (10 pg/ml) plus thrombin (1 pg/ml), on the other hand, stimulated chemotaxis by approximately 2.3-fold in the thrombin-activity-depleted assay system. Binding studies using [^{125}I]-thrombin revealed that the cells have specific saturable binding sites for thrombin. These results show that TM stimulates the invasive activity of MMT cells, probably by acting as a cofactor for the thrombin-stimulated invasion of the cells *via* its receptor and lowering the effective concentration of thrombin. The findings also indicate that the stimulation of invasive activity in the presence of 1% FCS and in the thrombin-activity-depleted assay system may mainly be mediated by the stimulation of chemotaxis.

Key words: invasion, thrombin, thrombomodulin.

Abbreviations: TM, thrombomodulin; MEM, modified Eagle's medium; CS, calf serum; FCS, fetal calf serum; MMP, matrix metalloprotease; ECM, extracellular matrix; Boc-Asp(Obzl)-pro-Arg-MCA, Boc-β-benzyl-Asp-Pro-Arg-4-methyl-coumaryl-7-amide; PBS, phosphate-buffered saline.

Thrombomodulin (TM) is a thrombin receptor on the surface of endothelial cells (*1*) that was first discovered as a cofactor for the thrombin-catalyzed activation of the anticoagulant protein C (*2*). Biologically active soluble forms of TM, which probably represent the products of limited proteolytic cleavage of cell-surface TM, were later detected in human plasma (*3*), suggesting a possible role of the soluble forms *in vivo*. TM also positively or negatively regulates various functions of thrombin as described below. TM stimulates the inactivation of pro-urokinase-type plasminogen activator (*4*), the activation of TAF I (*5*), and the activation of progelatinase A (*6*). TM inhibits the activation of platelets (*7*), the activation of factor X (*8*) and human endothelial cells (*9*), the stimulation of fibrin formation (*8*), and the proliferation of arterial smooth muscle cells (*10*) and human umbilical vein endothelial cells (*11*).

On the other hand, there are several direct and indirect lines of evidence indicating that thrombin stimulates invasion and/or metastasis by tumor cells (*12–18*), and it has recently been reported that the expression of TM is increased or decreased in some carcinomas. The expression of TM increases in squamous carcinomas of the lung (*19*), colorectal carcinomas (*20*), and some transitional

*To whom correspondence should be addressed. Tel: +81-3-3700-9347, Fax: +81-3-3700-9084, E-mail: niimi@nihs.go.jp

carcinomas (*21–22*), and its expression level is negatively correlated with the malignancy of carcinoma of the esophagus (*23*), hepatocellular carcinoma (*24*), and ovarian tumors (*25*). There is also evidence of increased serum levels of TM in some tumors, including pancreatic cancer (*26*), digestive tract carcinoma (*27*), and glioblastoma (*28*). Based on this evidence, it is likely that TM plays some role in the regulation of tumor metastasis.

In this study, we investigated the effects of TM on the invasive activity of a mouse mammary tumor cell line, MMT, by an *in vitro* invasion assay, because tumor cell invasion through the basement membrane is a critical step in the process of metastasis (*29–30*). We also compared the effects of TM with those of thrombin as a positive control.

MATERIALS AND METHODS

Materials—TM was a kind gift of Asahi Kasei Pharma, Japan. The TM was prepared as described by Gomi *et al.* (*31*). Plasmids containing the cDNA encoding TM (residues 1–498) were transfected into COS-1 cells, and the recombinant TM was purified from serum-free COS-1-cell-conditioned medium. The purified TM yielded a single band at 90 kDa in SDS-PAGE under reducing conditions. The recombinant TM was confirmed to be thrombin-free by a protein C activating assay developed in our laboratory (*32*). Thrombin (1,140 units/mg protein) was a kind gift of Mochida Pharmaceutical Co., Ltd., Japan. Hirudin was purchased from Wako (Osaka, Japan). A fluorogenic substrate, Boc-β-benzyl-Asp-Pro-Arg-4-methyl-coumaryl-7-amide (Boc-Asp(Obzl)-pro-Arg-MCA), was purchased from Peptide Institute, Inc. (Osaka, Japan).

Cell Culture—MMT mouse mammary tumor cells were obtained from the Japanese Health Science Research Resource Bank and cultured in modified Eagle's medium (MEM) supplemented with 10% calf serum (CS) on 60-mm diameter culture dishes, 4×10^5 cells per dish. After 7 d, the subconfluent MMT cells were detached from the culture dishes with 0.25% trypsin/EDTA, treated with MEM containing 10% CS, and collected by centrifugation. The cells were then washed with MEM and used in experiments. In some experiments, the thrombin activity associated with cells was depleted as described below, and the resultant cells were used for various experiments in which MEM containing 0.1% BSA was used as the basal medium. We refer to this assay system as the thrombin-activity-depleted assay system below. To deplete thrombin activity, the cell suspension (1.5×10^5 cells in 10 ml of MEM) was incubated in a non-adherent form on 100-mm diameter non-treated culture dishes pre-coated with BSA (10 mg/ml) for 2 h in a humidified chamber at 37°C under 5% CO_2, and then washed with MEM.

In Vitro Invasion Assay—In vitro invasion by MMT cells was measured in a Matrigel invasion chamber (Collaborative Biomedical Products, Bedford, MA, USA). The chamber (upper compartment) was placed in a 24-well culture plate (lower compartment), and the cell suspension (1.6×10^5 cells in 500 μl) and the basal medium (750 μl) containing various factors were added to the upper and lower compartments, respectively. MEM containing 1% fetal calf serum (FCS) or 0.1% BSA was used as the basal medium. Matrigel invasion chambers were precoated with fibronectin as described below before use in the thrombin-activity-depleted assay system. Human plasma fibronectin solution (IWAKI, Japan) was diluted to a final concentration of 5 μg/ml with phosphate-buffered saline (PBS), and a 300 μl aliquot was added to the chamber and a 750 μl aliquot to the 24-well culture plate. The chamber and 24-well plate were allowed to stand at 37°C for 2 h and were then washed with PBS. After incubating the cells for 18 h, the filters were fixed with methanol and stained with hematoxylin and eosin. The cells on the upper surface of the filters were removed by wiping with cotton swabs, and the number of cells that had migrated to the lower surface of the filters was counted under a microscope.

Measurement of Thrombin Activity—Thrombin activity in FCS, CS, and on cells was measured by the method of Kawabata *et al.* (*33*). A 10 μl volume of 10% FCS or CS was mixed with 90 μl of reaction buffer containing 50 mM Tris-HCl, pH 8.0, 100 mM NaCl, and 10 mM $CaCl_2$, with or without hirudin (0.5 unit/ml). Packed cells (1×10^6 cells) were suspended in 100 μl of reaction buffer with or without hirudin (0.5 unit/ml). After adding 1 μl of 10 mM substrate, Boc-Asp(Obzl)-pro-Arg-MCA solution to the cell suspension, the mixture was incubated for 20 min at 37°C, and the reaction was stopped by adding 600 μl of 0.6 M acetic acid. The fluorescence of the aminomethylcoumarine released was measured with a fluorospectrophotometer at an excitation wavelength of 380 nm and an emission of 460 nm. A blank solution was prepared by adding 1 μl of substrate solution to the reaction buffer mixed with 600 μl of 0.6 M acetic acid. Thrombin activity was calculated using 1, 2.5, 5 and 10 ng/ml thrombin solutions as standards and subtracting the fluorescence obtained in the presence of hirudin from that in the absence of hirudin. A linear dose-response curve was obtained between 0.5–5 ng/ml of thrombin, and its activity was inhibited by more than 98% by hirudin (0.5 unit/ml). The fluorescence of each sample was within the linear range.

Proliferation Assay—The cell suspension (1×10^5 cells in 4 ml) was seeded on 60-mm diameter culture dishes and incubated with each factor for 18 h. MEM containing 1% FCS was used as the basal medium. The cells were then detached from the culture dishes with 0.25% trypsin/EDTA, treated with MEM containing 10% CS, collected by centrifugation, and counted with a hemocytometer.

Adhesion Assay—Adhesion assays were performed by a modification of the method of Deryugina *et al.* (*34*). A 300 μl aliquot of fibronectin (5 μg/ml), prepared as described above, was added to each well of 24-well plates (IWAKI, Japan). The plates were allowed to stand overnight at 4°C, washed with PBS, blocked with 1% BSA in PBS for 1 h at 37°C, and finally washed in PBS. MMT cells (55×10^4 cells) were exposed to each factor in 2 ml of MEM containing 1% FCS for 30 min at 37°C. After washing with 2 ml of MEM, the cell suspensions (1×10^5 cells in 0.38 ml of MEM) were seeded on each well. After incubation for 30 min at 37°C, non-adherent cells were removed by washing with PBS, and the adherent cells were fixed and stained with 0.2% crystal violet in 10% ethanol for 10 min. After three washes with 2 ml of PBS,

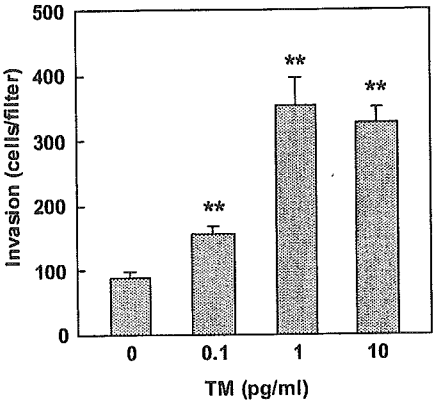

Fig. 1. **Dose dependency of the effect of TM on invasiveness.** MEM containing 1% FCS was used as the basal medium. The concentrations of TM indicated are the concentrations in the lower compartment. The data shown are means ± SD of the data obtained in duplicate wells in three experiments (**$p < 0.01$ *vs.* control). The deviation in each experiment was less than 10%.

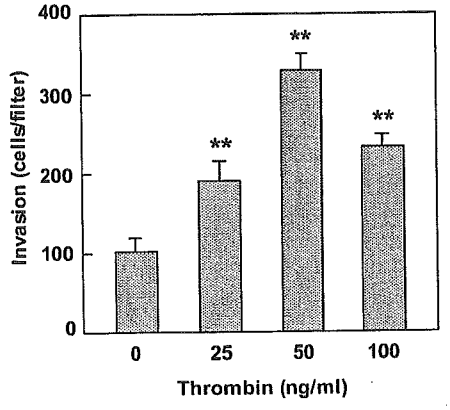

Fig. 2. **Dose dependency of the effect of thrombin on invasiveness.** MEM containing 1% FCS was used as the basal medium. The concentrations of thrombin indicated are the concentrations in the lower compartment. The data shown are means ± SD of data obtained in duplicate wells in three experiments (**$p < 0.01$ *vs.* control). The deviation in each experiment was less than 10%.

the dye was extracted in an end-over-end mixer with 600 μl of 50% ethanol in 50 mM sodium phosphate (pH 4.5) for 10 min, and absorbance was measured at 540 nm. The correlation between absorbance and cell number was confirmed in a preliminary experiment.

Chemotaxis Assay—Chemotaxis assays were performed with control inserts (Collaborative Biomedical Products, Bedford, MA, USA) in a similar manner to the invasion assay described above. The control inserts were not coated with Matrigel. MEM containing 1% FCS was used as the basal medium. The control inserts were pre-coated with fibronectin (5 μg/ml) as described for the pre-coating of the Matrigel invasion chamber in the thrombin-activity-depleted assay system.

Iodination of Thrombin and Determination of Binding—Thrombin was iodinated to a specific activity of 19.1 × 10^7 cpm/μg by the chloramine T method as described previously (*35–36*). After precoating 24-well plates with fibronectin (5 μg/ml) as described above, the cell suspensions (1.22 × 10^5 cells in 0.45 ml of MEM) were seeded into each well and incubated in a humidified chamber at 37°C under 5% CO_2 for 2 h. The cells were then washed with 0.4 ml of MEM containing 15 mM Hepes (pH 7.2) and 0.1% BSA and incubated for 1.5 h at 37°C in the same buffer with various concentrations of [^{125}I]-thrombin in the presence or absence of a 100-fold excess amount of unlabeled thrombin. After washing the cells four times with the same ice-cold buffer, the cells were solubilized with 0.4 ml of 1 N NaOH for 1 h at 37°C. Specific binding was calculated as the difference between total binding and nonspecific binding.

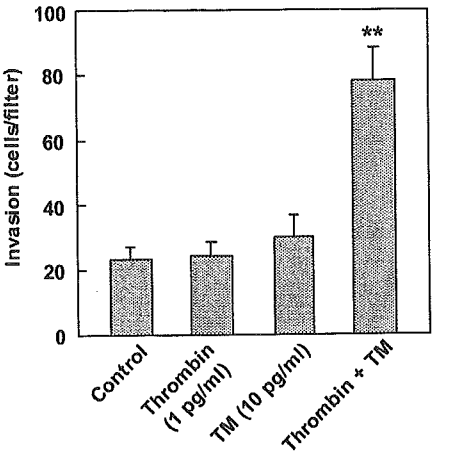

Fig. 3. **Effect of TM and thrombin on invasiveness in the thrombin-activity-depleted assay system.** Cells on which thrombin activity was depleted were used in the experiment. MEM containing 0.1% BSA was used as the basal medium. The data shown are means ± SD of data obtained in duplicate wells in three experiments (**$p < 0.01$ *vs.* control). The deviation in each experiment was less than 10%.

RESULTS

Effect of TM on Invasiveness—Figure 1 shows the effects of TM on the invasive activity of MMT cells in the presence of 1% FCS. TM significantly stimulated invasive activity in a dose-dependent manner, resulting in an approximately 3-fold stimulation at 1–10 pg/ml. Figure 2 shows the effects of thrombin used as a positive control. Thrombin also stimulated invasive activity in a dose-dependent manner.

On the basis of these findings, we investigated the possibility that the stimulation of invasion by TM might be dependent on thrombin that may have been introduced into the assay system as described below. First, thrombin activity in the assay system was measured. The thrombin concentrations in freshly prepared 10% FCS and CS measured by the thrombin activity assay were 200 pg/ml and 2.8 ng/ml, respectively. The amount of thrombin on the cells measured in a similar manner was 35 pg/10^6 cells. Based on these values, the thrombin concentrations in the assay system with or without 1% FCS were estimated to be 24.48 and 4.48 pg/ml, respectively. Second, the action of TM was examined in the thrombin-activity-depleted assay system described in "MATERIALS AND METHODS," and depletion of thrombin activity in the

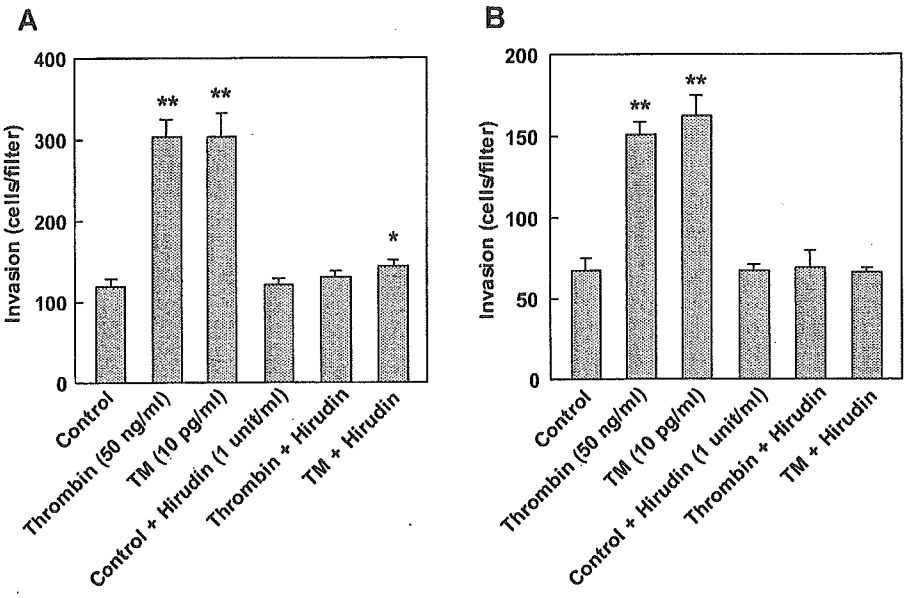

Fig. 4. **Effect of hirudin on the stimulation of invasion by TM.** (A) MEM containing 1% FCS was used as the basal medium. The indicated concentration of each factor is that in the lower compartment. The data shown are means ± SD of data obtained in duplicate wells in three experiments (*$p < 0.05$ *vs.* control; **$p < 0.01$ *vs.* control) (B) MEM containing 0.1% BSA was used as the basal medium. The data shown are means ± SD of data obtained in duplicate wells in three experiments (**$p < 0.01$ *vs.* control). The deviation in each experiment was less than 10%.

assay system was confirmed by the absence of any detectable thrombin activity on the cells. Figure 3 shows the effects of thrombin (1 pg/ml) and TM (10 pg/ml) on the invasive activity of cells in the thrombin-activity-depleted assay system. While neither thrombin or TM had any effect on invasion, TM plus thrombin stimulated invasion by approximately 3-fold.

Effect of Hirudin on the Stimulation of Invasion by TM—The action of TM was also examined in the presence of the specific thrombin inhibitor hirudin to investigate the possibility described above. Fig. 4, A and B, shows the effects of hirudin on the invasion-stimulating activity of TM in the presence and absence of 1% FCS. We used a 1 unit/ml concentration of hirudin in this experiment, because 50 ng/ml thrombin corresponds to 0.057 unit/ml, and so 1 unit/ml hirudin seemed adequate to inhibit this concentration of thrombin. As expected, hirudin (1 unit/ml) not only inhibited the stimulation by thrombin to control levels, but the stimulation by TM as well.

Effect of TM on Proliferation—Since tumor cell invasion consists of a series of events, including adhesion to the extracellular matrix (ECM) and chemotaxis, we investigated the effects of TM on these two events to clarify the molecular mechanism of the stimulation of invasive activity by TM. Before investigating the effect of TM on these processes, we investigated its effects on cell proliferation to confirm that the stimulation of invasive activity by TM is not an artifact of the enhancement of cell proliferation.

Figure 5 shows the effects of TM on MMT cell proliferation in the presence of 1% FCS. The numbers of cells in the presence of TM or thrombin did not differ from the numbers in the control cultures.

Effect of TM on Adhesion to Fibronectin—Figure 6 shows the effects of TM on adhesion to fibronectin, a basal lam-

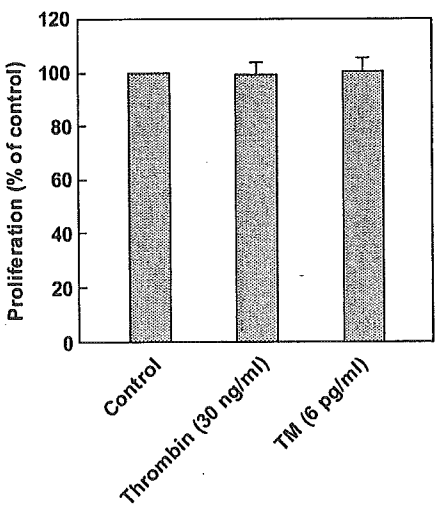

Fig. 5. **Effect of TM on proliferation.** MEM containing 1% FCS was used as the basal medium. The data shown are means ± SD of data obtained in duplicate dishes in three experiments. The deviation in each experiment was less than 10%.

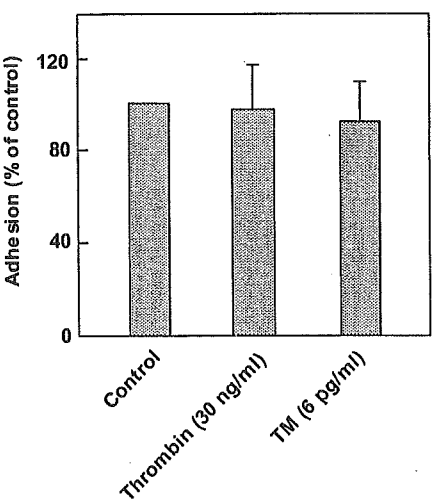

Fig. 6. **Effect of TM on adhesion to fibronectin.** MEM containing 1% FCS was used as the basal medium. The data shown are means ± SD of data obtained in duplicate wells in three experiments. The deviation in each experiment was less than 10%.